Proteolytic processing of LRP2 on RPE cells regulates BMP activity to control eye size and refractive error.

Ross F. Collery[1, 2], and Brian A. Link[1, †]

[1]Department of Cell Biology, Neurobiology and Anatomy,
Medical College of Wisconsin, WI 53226;
[2]Department of Ophthalmology and Visual Sciences,
Medical College of Wisconsin, WI 53226

Short title: Lrp2 cleavage and its effects on BMP signaling and eye size control

Keywords: Lrp2, SD-OCT, zebrafish, RNAseq, emmetropization, myopia

[†]Address correspondence to:
Brian A. Link, PhD
Department of Cell Biology, Neurobiology and Anatomy
Medical College of Wisconsin
WI 53226
Email: blink@mcw.edu
Phone: (414) 955-8072
FAX: (414) 955-6517

Abstract

Mutations in LRP2, a transmembrane receptor, cause ocular enlargement and high-myopia. LRP2 is expressed by the RPE and eye ciliary epithelia, binding many extracellular ligands, including Bmp4 and Shh. Signaling mediated by LRP2 is very context-dependent, and how multiple pathways are coordinated is unknown. Transcriptome analyses of ocular tissues revealed that controlled, sustained BMP signaling from the RPE is critical for normal eye growth and emmetropia (proper refraction). Using zebrafish, we demonstrate that BACE sheddase-dependent LRP2 cleavage produces a soluble domain that binds BMP4, inhibiting its signaling. We propose that controlled proteolytic cleavage of LRP2 makes two ligand-binding receptor forms available: a soluble BMP trap, and a membrane-bound RPE signaling facilitator. By modulating LRP2 cleavage, cells can fine-tune and coordinate multiple signaling pathways, as well as growth and turnover of the extracellular matrix, control of which is important to maintain proper eye size. This data supports the concept that LRP2 acts as a homeostasis node that buffers and integrates diverse signaling to regulate emmetropic eye growth.

Author Summary

For proper focusing and normal vision, the axial length of the eye needs to match the refractive power of the lens. This is achieved by fine-tuning multiple signaling pathways to regulate the shape of the eye primarily by remodeling of the sclera, the outermost layer of the eye. This process is termed emmetropization. Emmetropization cues are initiated by visual input, but how signals are transduced from the photoreceptors across the retinal pigment epithelium to the sclera is incompletely understood. Here we show that cleavage of Lrp2, a large receptor expressed on RPE cells in the eye, alters BMP signaling, which contributes to proper eye size control. Dysregulation of BMP signaling by a) absence of Lrp2 in mutant zebrafish or b) overexpression of BMP antagonists from the RPE both cause eye enlargement and myopia. Understanding how regulated cleavage of Lrp2 affects paracrine signaling provides critical insight to emmetropization, raising the possibility for development of therapeutic agents to combat the epidemic incidence of refractive error.

Introduction

LRP2/megalin is a large (>520 kD) transmembrane protein of the LDL-receptor related protein family that is expressed in retinal pigment epithelium (RPE) and ciliary epithelium of the eye (1–3), as well as on other absorptive epithelial cells such as proximal tubules in the kidney (4,5). Mutations in human *LRP2* lead to Donnai-Barrow syndrome, characterized by orbital hypertelorism, buphthalmia, high-grade myopia, agenesis of the corpus callosum, deafness, low molecular weight proteinuria and diaphragmatic hernia (6–8). Lrp2 binds a large number of proteins via four LDL type A domains. In the eye, Lrp2 has recently been shown to bind Sonic Hedgehog (Shh), preventing interaction with Patched1, and act as a clearance receptor to inhibit Shh signaling (9). In the absence of Lrp2, the optic cup margin shows extended proliferation, resulting in ciliary body hyperplasia. In the forebrain, however, Lrp2 functions as an auxiliary receptor with Patched1 to de-repress Smoothened activity and facilitate Shh signaling (10). Loss of Lrp2 in the forebrain results in holoprosencephaly and phenocopies Shh mutants. Forebrain deletion of Lrp2 also results in augmented BMP2/4/7 signaling (11). In that study, in vitro assays demonstrated Lrp2 can bind BMP4 and facilitate lysosomal degradation of the ligand. It is therefore clear that Lrp2 impacts signaling and homeostasis in context-dependent ways. As further example of the complexity of its regulation and function, LRP2 is cleaved in cultured kidney-derived cells by regulated intramembrane proteolysis (RIP), where the intracellular C-terminal domain can enter the nucleus and regulate gene expression (12,13). However, in vivo, over-expression of the C-terminus of Lrp2 in renal proximal tubules did not alter global gene expression nor result in obvious phenotype changes (14). Potentially, then, the extracellular domain may be the relevant bioactive fragment upon proteolytic processing. Indeed, soluble forms of LRP2 corresponding to extracellular fragments have also been reported, and are likely generated through cleavage at an extracellular site (15–19). Though the extracellular Lrp2-processing enzymes have not been identified, proteolysis has been predicted to be regulated by a sheddase (12). Since LRP2-mediated endocytosis is only known to occur when

membrane-bound, the potential function of soluble LRP2 is unknown. In this work, we uncover a role for extracellular and soluble versus membrane-bound Lrp2 where proteolysis acts as a possible molecular switch for BMP activity. Functional roles depend on the protein state: full length Lrp2 facilitates intracellular signaling required to prevent ocular overgrowth, while the cleaved, extracellular domain antagonizes BMP signaling by acting as a ligand trap and promotes axial lengthening.

Myopia is the most prevalent visual disorder in the world (20,21), and one of the leading causes of blindness in many countries, especially in south-east Asia. High myopia (generally regarded as requiring more than -6.0 diopters of lens correction) elevates the risk of retinal detachment, cataract and glaucoma, as well as myopic macular degeneration, chorioretinal atrophy and staphyloma (22,23). At least 33% of adults in the US are affected by myopia (24), and preventing progression of refractive error to high myopia helps to reduce the occurrence of these secondary pathologies. There are a large number of genetic factors that contribute to onset of myopia, with many proteins associated with extracellular matrix (ECM), the visual cycle, and neuronal development (25,26). In addition, myopia is linked to environmental factors, where excessive time spent indoors without exposure to bright outdoor light levels appears to increase the risk of developing myopia (27,28). However, much remains unknown about the nature and components of signaling pathways that are dysregulated in myopia, as well as the cellular sites of action.

Unlike many anatomical structures, the eye has an absolute requirement for precise size control, since even small deviations in axial length have dramatic effects on refractive state. Small changes in axial length associated with genetic mutation or dysregulation of gene expression can have significant effects on refractive state, while only subtly affecting eye size. Continuous control of eye size to establish and maintain emmetropia after juvenile development has been demonstrated as necessary in all species studied (reviewed in (29)). Early post-natal eyes are ametropic, and visual cues inform the eye how to correct refractive errors. Signaling within the eye that mediates emmetropization is poorly

understood, both in terms of the cells involved and the precise pathways utilized. Dysregulation of these pathways however, can lead to significant refractive error.

Mutations in BMP4 have been associated with a spectrum of ocular disorders, including high myopia. Individuals from families that frequently presented with anophthalmia-microphthalmia, retinal dystrophy, myopia, brain malformation and poly/syndactyly were found to have a nonsense frameshift mutation in BMP4 that segregated with these symptoms (30,31). Genome wide association studies (GWAS) identified linked DNA variants located near human *BMP2* and *BMP3* in myopic individuals (25,26). In animal studies, myopia induced by form-deprivation resulted in reduced BMP signals. In chicks, induced myopia led to a reduction in BMP2 in the retina/RPE (32), while in guinea pigs, form-deprivation myopia resulted in a reduction in BMP2 and BMP5 within the sclera (33,34). Similarly, defocus-induced myopia in guinea pigs caused a decrease in BMP2 in the sclera (35), and a decrease in BMP2/4/7 in the RPE (36,37). Conversely, lens-induced hyperopia has been shown to cause an increase in BMP2/4/7 in the chick RPE (36,37). Finally, prematurely-truncating mutations in the BMP antagonist Noggin causing NOG-related-symphalangism spectrum disorder/stapes ankylosis have been associated with hyperopia (38–40). Taken together, these data indicate a strong connection between BMP signaling and refractive error, where reduced BMP levels associate with myopia or lengthening of the eye, and increased BMP levels associate with hyperopia or shortening of the eye.

BMP ligands are members of the TGFβ superfamily whose receptors transduce signaling events from the cell surface to activate Smad and non-Smad signaling, as well as non-transcriptional responses (for review, see (41)). Prior to binding to the transmembrane receptors, BMPs can be bound by secreted, soluble ligand trap antagonists such as Noggin, which bind BMPs and prevent interaction with their receptors by acting as antagonists (42).

We have previously described a zebrafish *lrp2* mutant model, which shows enlarged eyes and high myopia, as well as elevated IOP and retinal ganglion cell damage (43,44). In this work, we profile

123 gene expression in ocular tissues of wild-type and *lrp2*$^{-/-}$ mutants at the onset of buphthalmia. We show
124 that eye enlargement and myopia can be ameliorated in *lrp2*$^{-/-}$ zebrafish mutants by expressing full-
125 length Lrp2 in the RPE, indicating that Lrp2 acts locally within the eye to control emmetropization. We
126 also demonstrate that Bmp4 binds to the first of the four LDL type A domains of Lrp2. To begin to
127 address the role of cleaved and released extracellular Lrp2, we directed RPE-specific overexpression of
128 Noggin3 (a high affinity BMP antagonist) and Gremlin2 (a lower affinity BMP antagonist). These studies
129 showed that inhibiting BMP signaling leads to eye enlargement and myopia. Of particular relevance, we
130 find that overexpressing a secreted version of the first LDL type A domain of Lrp2 from the RPE
131 phenocopies the effects observed with the known BMP antagonists and exacerbates myopia in *lrp2*
132 mutant zebrafish. We also demonstrate that extracellular cleavage of zebrafish Lrp2 occurs in cultured
133 human cells, and find that cleavage is regulated by a beta-site amyloid precursor protein cleaving
134 enzyme (BACE) protease. Furthermore, inhibition of BACE enzyme activity in the zebrafish eye increases
135 Bmp signaling in the choroid/sclera, the primary region of extracellular remodeling associated with
136 emmetropic growth. Similarly, expression of a constitutively soluble LDLA1 domain from the RPE
137 reduces BMP activity, while expression of a membrane-bound form does not. Analysis of *lrp2*$^{-/-}$ and wild-
138 type eye transcriptomes shows altered expression of ECM components. We propose that modulation of
139 Bmp signaling, facilitated by Lrp2 and its cleavage state, contributes to controlling eye size and prevents
140 aberrant growth and myopia.
141
142
143

Results

Loss of Lrp2 results in alterations to multiple signaling pathways within the eyes

Loss of function mutations of *lrp2* lead to enlarged, myopic eyes in zebrafish and other species (6,7,43,45). However, the effect of disrupting Lrp2 activity on specific signaling pathways and cellular processes has not been extensively assessed in ocular tissues. Because ocular histology and growth is normal at 1 mpf and earlier in *bugeye* fish (46), we performed transcriptome analyses at this stage to avoid potential confounding secondary and/or pathology-related pathway changes that occur in more aged animals. Specifically, we isolated RNA from 1 mpf wild-type and *lrp2*$^{-/-}$ eyes, as well as dissected ocular tissues (sclera/choroid, RPE, retina), where each condition was replicated in triplicate with independent biological samples. RNA extracted from these samples was assayed for tissue specificity using retinal-, RPE- or sclera/choroid-specific marker genes by qPCR (S1 Figure), and then processed for deep RNA sequencing (RNAseq) (S1 Table, S2 Table). Subsequent bioinformatic analysis was applied to detect potential changes in signaling pathways associated with loss of Lrp2.

Using curated databases, such as Gene Ontology, DAVID, KEGG, and IPA, for transcript signatures associated with different types of signaling, we assessed whether genes altered by loss of Lrp2 correlated with those of specific pathways. Analyses indicated that Bmp and Shh signaling were both altered in *lrp2* mutant eyes (S3 Table). However, expression signatures associated with these databases are assembled from published data derived from non-ocular tissues of non-zebrafish origin. Since Bmp and Shh signaling pathways are strongly associated with control of eye size and development, and both have been previously shown to be regulated by Lrp2, we generated ocular-specific, zebrafish transcript signatures for Bmp and Shh. This was accomplished by using transgenic zebrafish lines to acutely overexpress either Shha or Bmp4 under inducible heat-shock control. At 5 dpf, lines *hsp70l:shha-eGFP* (47), or *hsp70l:eGFP-bmp4* (this study) were heat-shocked before isolation of GFP-positive eyes 8 hours

later. RNA expression profiles from these eyes were used to define zebrafish ocular responses to Shh and Bmp pathway activation (S2 Figure, S3 Figure).

These signatures were used to carry out gene-set enrichment analysis (GSEA) and assess overlap of the gene sets in Lrp2-deficient ocular tissues (see below). GSEA examines transcriptome datasets to determine whether a defined list of genes (referred to as signatures or commonly-regulated gene sets) is concordantly and statistically altered between control and experimental groups (48,49). Specifically, RNA profiles of whole eye and dissected ocular tissues from 1 mpf wild-type and *lrp2*$^{-/-}$ mutant zebrafish were compared to eye-specific Bmp4 and Shh reference gene sets. Both pathways were significantly altered in the absence of Lrp2. To prioritize the gene pathway and eye tissue of greatest importance, we applied a simple scoring system to assess the significance of Lrp2 for each pathway in specific eye tissues (Table 1). For each sample assessed, nominal GSEA p-values lower than 0.05 were scored as +1, while p-values greater than 0.05 were scored as 0. The final scores were summed and used to rank significance of each signaling pathway in each tissue. We found the Shh pathway was broadly affected and scored highest for whole eyes. Bmp pathway genes were more selectively altered within the RPE, but also showed changes in the sclera/choroid and neural retina. Because Shh has already been studied in the context of eye size regulation using mice (9), and RPE is known as a key signaling tissue for emmetropization and thought to mediate signals processed in the sclera and choroid, we concentrated our analysis on Bmp signaling associated with those tissues.

RPE-driven expression of Lrp2 partially rescues the buphthalmic *bugeye* phenotype

To investigate whether buphthalmia was caused by absence of Lrp2 from the eyes, which is expressed in the RPE, or by systemic changes in circulating ligands normally bound by Lrp2 in the kidney and elsewhere, we developed an RPE-specific promoter to express Lrp2 only in that tissue. Similar to studies using mammalian *RPE65*, we isolated approximately 800 bp upstream of the translational start

site of zebrafish *rpe65a* (50). We found that this promoter drove fluorescent transgene expression in developing and adult RPE and pineal (Figure 1). In embryos, *rpe65a:eGFP* transgenic expression was broad, but low. In larvae, we observed strong enrichment of fluorescent expression in developing RPE cells starting just prior to when they resolve to a monolayer (51). Subsets of cells within the pineal also showed enriched eGFP expression. In adult zebrafish, eGFP expression was maintained and restricted to the RPE and pineal.

We next isolated the full-length zebrafish *lrp2* coding sequence and generated transgenic lines expressing both *rpe65a:Gal4* and DsRed ←*UAS* →Lrp2-HA (abbreviated to *rpe65a>lrp2-HA*). This transgenic line uses the *rpe65a* promoter to drive Gal4 expression, which transactivates the upstream activating sequence (UAS) bi-directionally so that fluorescent DsRed marks cells co-expressing Lrp2-HA. At 3 mpf, wild-type and *lrp2*$^{-/-}$ fish with or without RPE-driven Lrp2-HA expression were examined using spectral domain - ocular coherence tomography (SD-OCT) to assess eye size relative to body axis and calculate the relative refractive error, a measure of deviation from emmetropia. This imaging technique allows for precise measurements in live samples, avoiding tissue fixation artifacts and enabling detection of the small differences in axial length that have major impact on visual blur (52). Adult *lrp2*$^{-/-}$ mutant zebrafish carrying the *rpe65a>lrp2-HA* transgenes had significantly smaller eyes (lower eye axial length: body axis ratios) than non-transgenic, mutant siblings (Figure 2 A). However, *lrp2*$^{-/-}$ *rpe65a>lrp2-HA* eyes still had significantly larger eyes than wild-type controls. Likewise, *lrp2*$^{-/-}$ adult zebrafish carrying the *rpe65a>lrp2* transgenes had significantly reduced relative refractive errors (less myopic) when compared to non-transgenic, mutant siblings (Figure 2 B). Similar changes were measured in replicate experiments. Furthermore, expressing Lrp2 directly from the *rpe65a* promoter also resulted in abatement of enlarged eyes and myopia (data not shown). Importantly, the *rpe65a* promoter does not show activity within the ciliary margin zone (Figure 1 G), and so the rescue measured is due only to RPE cell expression and not

from the ciliary region, which is known to have strong Shh activity. In summary, this data indicate that RPE-expressed Lrp2 contributes to regulation of eye growth and emmetropization.

eGFP-Bmp4 is functional and perdures in discrete locations during development

Because eye size and refraction were rescued by RPE-expression of Lrp2 within *lrp2* mutants, and *lrp2* mutant RPE showed defects in BMP signaling, we sought to explore more directly the relationship of Lrp2 and BMP activity using an eGFP-tagged Bmp4. To validate that eGFP-Bmp4 was functional, we generated a transgenic line, *hsp70l:eGFP-bmp4*, that placed the Bmp4 fusion protein downstream of a heat shock-inducible promoter, allowing activation of eGFP-Bmp4 expression at various times during development. Heat-induced eGFP-Bmp4 expression was verified by Western blot (S4 Figure). Secretion and activity was confirmed by inducing global eGFP-Bmp4 expression at 30 – 50% epiboly, which resulted in extracellular eGFP and severe ventralization phenotypes, similar to the patterning defects observed in zebrafish following overexpression of native Bmp at these early times (53).

At embryonic stages after axis patterning, expression of eGFP-Bmp4 resulted in milder phenotypes. Expression induced at 1, 2, 3 or 4 dpf followed by image analysis 24 hours later revealed patterns of perdurance of eGFP-Bmp4. Stabilized eGFP-Bmp4 was enriched in cells of the eye, head, somites and other areas (S4 Figure). Despite the mild phenotypic consequences at later stages, eGFP-Bmp4 expression did stimulate Smad signaling, as shown by elevated red fluorescence from the BRE:dmKO2 reporter (54). These data verify the bioactivity of eGFP-Bmp4.

Given the association between Bmp4 levels and refractive state of the eye, we attempted to overexpress Bmp4 from the RPE. To do so, we generated a *UAS:eGFP-bmp4* transgenic line to combine with the *rpe65a:Gal4* transgene and achieve sustained RPE-derived overexpression of eGFP-Bmp4. However, *rpe65a* and our promoter transgene expresses broadly during early development before it

238 becomes confined to the RPE and pineal, resulting in severe microphthalmia ((55), this study).
239 Interestingly, these embryos often developed into adults with abnormal phenotypes restricted to the
240 eyes, including coloboma and disorganization of the retina (S5 Figure). Since the eyes did not develop
241 correctly, we were unable to use this strategy to isolate the effects of Bmp4 overexpression on ocular
242 size and the refractive state.
243
244 **Overexpression of BMP ligand-trap antagonists from the RPE alter eye size and cause myopia**
245 To test whether BMP activity associated with the RPE is critical for eye growth and
246 emmetropization, we overexpressed the potent Bmp antagonist zebrafish Noggin3 (Nog3) from that
247 epithelium. We initially tried to create a double transgenic line that bi-directionally expresses *DsRed←*
248 *UAS→nog3* within a stable *rpe65a:Gal4* line. Despite repeated attempts, we were unable to establish
249 founder fish that gave rise to offspring transgenic for both constructs, likely due to deleterious effects of
250 expressing Noggin3 broadly during early development, as was the case for Bmp4 overexpression (S5
251 Figure). Instead, we injected the plasmid carrying the *DsRed←UAS→nog3* sequence into *rpe65a:Gal4*
252 embryos (either *lrp2*$^{+/-}$ as sibling controls, or *lrp2*$^{-/-}$ mutants) and screened for red fluorescence
253 expression in RPE cells at 5 dpf. These fish, abbreviated *rpe65a>nog3*, were raised to adulthood, and eye
254 and body metrics measured at 2 months.
255 Overexpression of Nog3 in RPE of *lrp2*$^{-/-}$ zebrafish exacerbated the enlarged eye phenotype and
256 enhanced the degree of myopia as compared to non-transgenic siblings that were also mutant for *lrp2*
257 (Figure 3 A, B). Interestingly, overexpression of Nog3 in *lrp2*$^{+/-}$ zebrafish, which are indistinguishable
258 from wild-type fish, induced eye enlargement and refractive errors. These results show that RPE-based
259 overexpression of Nog3 increases the degree of myopia in *lrp2*$^{-/-}$ adult zebrafish, and causes myopia in
260 *lrp2*$^{+/-}$ zebrafish that are otherwise slightly hyperopic.
261

To complement the Noggin3 studies and attempt to generate stable transgenic fish capable of expressing a BMP antagonist, we tested the effects of a weaker BMP-binding inhibitor, Gremlin2, on eye size and refractive state. Indeed, we were able to generate double transgenic lines of *rpe65a:Gal4; DsRed←UAS→grem2* (abbreviated to *rpe65a>grem2*). These fish overexpress Grem2 from the RPE, and show normal survival and fertility. Overexpression of Grem2 from *lrp2*$^{-/-}$ RPE cells increased the relative ocular axial length (Figure 3 C). The mean relative refractive error was also significantly affected (Figure 3 D). However, in *lrp2*$^{+/-}$ zebrafish, overexpression of Grem2 did not significantly alter eye size or impact the refractive state. Cumulatively, these data are consistent with the concept that modulation of BMP signaling within the RPE and adjacent tissues can regulate ocular growth and emmetropization.

Bmp4 binds to the LDLA1 domain of Lrp2 in vivo

Bmp4 has previously been shown to bind purified Lrp2 in vitro, though the site of interaction has not been discovered, and direct interaction has not been verified on cells (56). The extracellular portion of Lrp2 can be divided into four domains, characterized by LDLA motifs. We generated four expression vectors corresponding to the isolated LDLA domains 1-4, and individually fused each domain with an S•tag epitope in plasmids CMV/SP6:LDLAn-S•tag, where n corresponds to LDLA domain 1, 2, 3 or 4. In addition we constructed an epitope-tagged Bmp4 to investigate whether, and to which domain of Lrp2, BMP4 binds in vivo (S4 Figure).

Zebrafish Lrp2 LDLA domains 1 through 4 were transfected along with eGFP-tagged Bmp4 into HEK293T cells. LDLA domains were immobilized from conditioned medium and extracted cellular proteins before probing for bound eGFP-Bmp4 by Western blot. Comparing total input protein against protein retained after immunoprecipitation showed that eGFP-Bmp4 binds to the LDLA1 domain, but not to LDLA domains 2, 3 or 4 (Figure 4). Importantly, binding of ligands to extracellular regions of Lrp2,

which may be cleaved from the cell surface, suggests that Lrp2 might act as a ligand trap as well as an endocytic receptor.

RNAseq shows altered gene signaling in dissected eye tissues of *lrp2*$^{-/-}$ and wild-type

To evaluate which Bmp ligands and receptors are available for signaling in the RPE and adjacent tissues, we evaluated RNAseq data from wild-type 1 mpf eyes and dissected tissues (S6 Figure). Most Bmp ligands were more highly expressed in RPE and choroid/sclera than retina or whole eye (one-way ANOVA with Tukey's multiple comparison test), though we note that *bmpr2a*, *bmpr2b* and *acvr2aa* are more highly expressed in the retina than elsewhere. The Bmp receptors *bmpr1ab* and *bmpr1ba* were more highly expressed in the RPE than other tissues, and *bmpr1ab* was also enriched in the sclera/choroid. Activin receptors, which can also transduce Bmp signals as well as other TGFβ superfamily signals, were more broadly expressed in all eye tissues, though *acvrl1/alk1* and *acvr1l/alk2/alk8* were enriched in the RPE. We note that Bmp type II receptors (*bmpr2a*, *bmpr2b*) can complex with Alk1 (AcvrL1) and Alk2 (Acvr1) as well as Bmp type I receptors, and it may be that TGFβ signaling unrelated to Bmp signaling is the reason for high levels of *bmpr2a* and *bmpr2b* in the retina. Taken together, these data suggest that Bmps are important for signaling between the RPE and sclera/choroid, consistent with a model in which Bmp activity mediates the ability of RPE to direct emmetropic remodeling of the sclera/choroid.

Secretion of the LDLA1 domain of Lrp2 from the RPE increases myopia in an *lrp2*$^{-/-}$ zebrafish

Because full-length Lrp2 overexpression reduced the large eye phenotype in *lrp2*$^{-/-}$ zebrafish, and Bmp4 bound only to LDLA1, we wanted to test whether expression of the LDLA1 domain alone from

the RPE was sufficient to rescue the *bugeye* phenotype. We placed DNA encoding the LDLA1 domain downstream of the native Lrp2 signal peptide to ensure proper export of the resulting protein. Using this plasmid, we made the following transgenic line: *DsRed←UAS→lrp2,signal peptide-LDLA1* (abbreviated to *rpe65a>LDLA1*). These fish were combined with *rpe65a:Gal4* carriers to overexpress the secreted N-terminal domain of Lrp2 (signal peptide-LDLA1) from the RPE. Double transgenic progeny grew to maturity and were fertile. Overexpression of the Lrp2 LDLA1 domain from the RPE of *lrp2*$^{-/-}$ mutants increased both the normalized eye size and relative refractive error compared to mutant siblings that only expressed Gal4 (Figure 5 A, B). However, overexpression of LDLA1 did not significantly affect the eyes of *lrp2*$^{+/-}$ zebrafish. These results show that overexpression of RPE-secreted Lrp2 LDLA1 domain increases the degree of myopia in *lrp2*$^{-/-}$ adult zebrafish, similar to the results found with overexpression of either Nog3 or Grem2.

Lrp2 is cleaved extracellularly to release a soluble domain

Replacement of full-length Lrp2 in the *lrp2* mutant RPE reduces the severity of the buphthalmic phenotype; however, overexpression of the secreted, Bmp4-binding domain exacerbates eye enlargement. This suggests that soluble Lrp2 has a different function versus membrane-bound Lrp2, and that release of the extracellular domain by proteolytic cleavage may act as a functional switch. In the eye, proteolysis of Lrp2 may serve to fine-tune signaling that controls emmetropization. In cultured proximal tubule cells of the kidney, LRP2 has been shown to be cleaved to produce a soluble extracellular N-terminal domain and an intracellular C-terminal domain. To examine the possibility of extracellular cleavage of zebrafish Lrp2, and investigate the factors that modulate this event, we generated a plasmid that placed secreted eGFP (seGFP) upstream of a 691 amino acid fragment of Lrp2 (457 a.a. extracellular domain + 234 a.a. of the full transmembrane and intracellular domains), and placed mCherry at the C-terminus to make *seGFP-lp2 (ECD/ICD)-mCherry* (Figure 6 A). This dually-tagged

lrp2 fragment was put under the control of a CMV promoter and expressed in HEK293T cells. Conditioned culture medium was harvested after 48 hours following transfection of the plasmid and the Lrp2 epitopes were probed by Western blot. As controls, *seGFP-V2A-mCherry* (constitutive cleavage) and *seGFP-mCherry* (no cleavage) were also placed under the control of the CMV promoter and transfected into equivalent batches of cells.

To investigate regulation of extracellular cleavage, and to gain insight into the class of proteases that might mediate cleavage, we used pharmacological agents known to affect the activity of different classes of sheddases. The plasmid *CMV:seGFP-Lrp2 (ECD/ICD)-mCherry* was transfected into HEK293T cells for 24 hours, before cells were treated with a variety of compounds that either inhibit or promote extracellular cleavage of LDL receptor family members. To inhibit sheddases, matrix metalloprotease inhibitor III, TAPI-0 or LY2811376 were used to block activity of matrix metalloproteases, TNF-α converting enzyme (TACE)/ADAM17, and BACE1, respectively. To augment sheddase activity we added phorbol 12-myristate 13-acetate (PMA) and sodium maleate, which are known to stimulate cleavage of amyloid precursor protein. Transfected cells were treated with compounds for 24 hours before conditioned medium was collected. Conditioned medium from each group was applied to anti-GFP-conjugated agarose to bind any Lrp2 that may have been released into the medium through cleavage (seGFP-Lrp2 ECD), or potentially exocytosis or cell lysis (*seGFP-Lrp2 (ECD/ICD)-mCherry*) (Figure 6B). Bound proteins were eluted from the agarose and detected by Western blotting using anti-eGFP antibody (JL-8). Of the compounds tested, only LY2811376 altered the amount of eGFP-containing proteins in the medium, suggesting that BACE1 (or a similar enzyme that is also inhibited by LY2811376) mediates extracellular cleavage of Lrp2 (Figure 6 C). To further confirm BACE1-mediated cleavage of Lrp2, the experiment was repeated in duplicate, with culture medium collected before (24 hours after transfection) and after (48 hours after transfection) drug administration (Figure 6 D). Following LY2811376 treatment, when the amount of eGFP-containing proteins was normalized to pre-drug levels,

there was an ~40% average reduction in extracellular cleavage observed (Figure 6 E). These results indicate that release of the extracellular region of zebrafish Lrp2 is mediated in part by a BACE1-like activity, and the responsible protease(s) may modulate Lrp2 function in vivo. Consensus substrate sites for BACE enzymes have been published, and comparisons with zebrafish Lrp2 protein sequence suggests several sites for BACE enzyme activity (S7 Figure). Our results so far suggest that BACE enzyme(s) are capable of extracellular cleavage of ectopically expressed Lrp2 and the released LDLA1 domain can bind Bmp and affect signaling.

Inhibition of BACE activity increases Bmp signaling in tissues basal to the RPE

We next tested whether inhibiting BACE activity affects Bmp signaling in vivo using zebrafish. To inhibit BACE activity, we used two potent compounds, LY2811376 and BACE inhibitor II. Larval zebrafish transgenic for the Bmp-response element:d2GFP (*BRE:d2GFP*) express destabilized GFP to report the location and level of Bmp signaling in vivo (57). *BRE:d2GFP* larvae were treated at 4 dpf for 24 hours with a) 150 µm LY2811376 (BACE1 inhibitor), b) 50 µm BACE inhibitor II, or c) DMSO vehicle as control. At 4 dpf, zebrafish eyes show highest Bmp activity in the outermost layers (RPE, choroid, sclera) (Figure 7A). Following drug or vehicle treatment, eyes of *BRE:d2GFP* larvae were imaged by fluorescent microscopy and the signal in the outer layers of the eye was quantified. BACE inhibitor drug treatments led to higher levels of Bmp signaling in outer layers of reporter zebrafish when compared to vehicle controls for both LY2811376 and BACE inhibitor II (Figure 7 A, B, F, G).

To clarify the specific identity of the outer layers of the eye demonstrating augmented Bmp signaling in response to BACE inhibition, we incrossed *BRE:d2GFP* and *rpe65a:mCherry-CAAX* zebrafish and examined doubly transgenic larvae at 4 dpf. Green fluorescent tissue layers were found to lie outside

the red fluorescent marked RPE layer (Figure 7 C - E), indicating that the sclera/choroid layers are responsible for the altered BMP signaling following inhibition of BACE enzyme activity.

Expression of soluble, but not membrane-bound, Lrp2 LDLA1 domain from the RPE reduces choroidal/scleral Bmp activity

In order to investigate whether cleavage of Lrp2 from membrane-bound to soluble form affected its ability to modulate Bmp signaling, we made plasmids *rpe65a:lrp2 LDLA1-eGFP* and *rpe65a:lrp2 LDLA1-ICD-eGFP* that drive expression of either soluble Lrp2 LDLA1 or membrane-bound Lrp2 LDLA1 with its native transmembrane domain, respectively. These plasmids were separately injected into BRE:dmKO2 reporter zebrafish, and Bmp activity levels measured in the eye at 5 dpf by fluorescence quantification. In BRE reporter fish, fluorescence is almost completely confined to the choroid/scleral layers (see previous section). When compared with uninjected control *BRE:dmKO2* eyes, soluble Lrp2 LDLA1 reduces Bmp activity significantly, while membrane-bound Lrp2 LDLA1 has did not affect reporter activity (Figure 8). This indicates that soluble LDLA1 can act as an inhibitor for Bmps, preventing them from binding and signaling through appropriate receptors, while membrane-bound LDLA1 does not interfere with Bmp signaling, but potentially augments other pathways within RPE cells..

***lrp2*$^{-/-}$ zebrafish eyes have elevated transcription of ECM components and modulating genes**

Associations between refractive error and genes involved in ECM growth and remodeling have been reported in individual gene studies, and in genome-wide association studies (25,26,58–64). In the eye, BMPs have been shown to inhibit excessive TGF-β2 induction of ECM proteins (65–69). Since we have shown that absence of Lrp2 leads to modulation of genes influenced by Bmp overexpression, we hypothesized that Lrp2 may assist in fine-tuning Bmp levels to properly control deposition and turnover of ECM proteins. GSEA analysis of *lrp2*$^{-/-}$ and wild-type eyes at 1 mpf showed upregulation of ECM

components and modulators when queried using ECM-receptor interaction pathway signature (KEGG pathway hsa04512; gene names converted from human to zebrafish) (Figure 9). This suggests that Lrp2 is necessary in the eye to maintain appropriate levels of ECM proteins in the eye, and that ECM protein dysregulation may result in the excessive eye growth seen in *lrp2/bugeye* mutants.

Discussion

Mutations in Lrp2 cause excessive eye growth and myopia; however, the nature of the influence of Lrp2 on ocular globe size and emmetropization is likely multifactorial and has not been fully elucidated. Here we show that transgenic expression of recombinant, full length Lrp2 from the zebrafish RPE can significantly reduce the *lrp2* mutant phenotype, demonstrating that the effects of Lrp2 are at least partly local to the eye, and not exclusively the result of systemic factors that circulate in the blood or lymphatic systems. This interpretation is consistent with recent studies of mice with *foxg1*-mediated inactivation of Lrp2, which eliminates expression from the neural retina, RPE, and forebrain and caused eye enlargement and myopia (70). Using transcriptomic analyses, we found deletion of Lrp2 altered Bmp signaling, as well as other pathways. Because of the specificity of perturbed Bmp signaling to the RPE and sclera/choroid, coupled with previous studies implicating BMP signaling in emmetropization, we focused subsequent experiments on how Lrp2 regulates this pathway. Our studies indicate that Lrp2 can be cleaved from the RPE to release an extracellular domain capable of binding and inhibiting Bmp4 activity, and potentially activity mediated by other Bmps. Indeed, RPE expression of the Lrp2 LDLA1 domain mimicked the effects of known BMP2/4/7 ligand trap antagonists to promote eye size and myopia. Application of sheddase inhibitors to zebrafish larvae suggests that the Lrp2 extracellular domain is released from the basal side of the RPE, adjacent to the sclera /choroid, and cleavage is mediated by BACE activity. The Lrp2 sheddase, therefore, acts as a molecular switch to convert the full-length Lrp2 protein from a potential facilitator of Bmp signaling and modulator of other pathways, to a

soluble antagonist of Bmp signaling. Cumulatively, this suggests that regulated cleavage of Lrp2 enables fine-tuning of multiple pathways to control ocular growth and emmetropization. We propose a model where wild-type eyes balance cleavage of Lrp2 from a membrane-bound to a soluble form thus fine-tuning Bmp signaling. When Lrp2 is completely absent, signaling pathways augmented by membrane-bound Lrp2, such as BMP, Shh, and perhaps others, can no longer be facilitated, leading to reduced activity and excessive eye growth (Figure 10). This disease phenotype can be further exacerbated by transgenic expression of soluble Lrp2 LDLA1 which acts as a decoy for Bmp ligands, decreasing signaling further and causing greater eye growth.

Complexity in Lrp2 function is underscored by its effect on multiple pathways, but also on its distinct actions in different tissues. For example, in addition to altered Bmp signaling, loss of Lrp2 in zebrafish also affects Shh signaling in the eye. Our observed changes in Shh signaling with zebrafish are consistent with recent analysis of the retinal margin in *Lrp2* mutant mice (9). This study showed elevated Shh activity and subsequent hyperplasia of the ciliary epithelium. Expansion of the ciliary epithelium is also observed in zebrafish (43). In both mice and zebrafish with *lrp2* mutations, neural retinal growth, however, is insufficient for the size of the eye enlargement and the neuronal layers become stretched and thin prior to detected degeneration of ganglion cells. These observations suggest that Shh contributes to buphthalmia by promoting proliferation of the ciliary epithelium, which consequently increases aqueous humor production, and that fluid pressure promotes expansion of the ocular globe. Distinct from Lrp2 function in the ciliary epithelium, our data indicates RPE-localized Lrp2 modulates signaling that ultimately controls extracellular remodeling associated with the sclera and choroid which is known to underlie axial length changes.

Potentially, tissue-specific functions of Lrp2 may depend on the presence of ligands and expression of other cell surface (co-)receptors, as well as sheddase activity. As previously demonstrated, cellular

and tissue context governs whether Lrp2 positively or negatively impacts Shh signaling (9,10,56). Lrp2 in the forebrain serves as a Patched co-receptor to augment Shh activity, while in the ciliary epithelium Lrp2 mediates Shh endocytosis and lysosomal shuttling to temper Shh activity. Similar complexity is emerging with the influence of Lrp2 on Bmp signaling. Previously, it has been demonstrated in forebrain ventricular cells that full-length Lrp2 can also endocytose and facilitate lysosomal degradation of Bmp4 (56). Conversely, full-length Lrp2 on RPE cells may function to augment Bmp activity within those cells. In vascular endothelial cell precursors, the highly homologous Lrp1 can function as a co-receptor with Alk6/BmpRII for Bmp4 to promote holocomplex endocytosis to prolong and enhance Bmp signaling (71). This possibility is consistent with a requirement of Bmp activity implicated by myopia-associated variants that affect genes encoding ligands, receptors and regulators of Bmp signaling. Our studies indicate that cleavage of Lrp2 would disrupt full-length function(s) and convert the extracellular domain to a Bmp ligand trap antagonist. In this manner, then, the fraction of uncleaved Lrp2 on RPE cells could autonomously augment Bmp signaling, while shed extracellular protein would non-autonomously temper Bmp signaling in the sclera and choroid. Proteolytic processing would also affect Shh signaling by preventing the full-length functional influence of Lrp2 on that pathway.

Our discovery that the shed extracellular domain of Lrp2 is functional has several implications. First, modulation of the BACE(-like) sheddase might serve as a therapeutic target for pathological, progressive myopia. However, the BACE1 inhibitor LY2811376 has been shown to cause retinal dystrophy in rodents (72,73). Similarly, genetic deletion of BACE1 in mice resulted in significant choroidal, RPE, and retinal pathology (73). As BACE proteases are known to process many different proteins, any therapeutic approach to modulate Lrp2 cleavage would need precision. Related to cleavage of the Lrp2 extracellular domain, it is interesting to note that mouse models of Lrp2 knockout show different phenotypes depending on the mutant allele: homologous recombination to replace 1.5 kb of the *Lrp2* gene with a neomycin cassette results in near-total embryonic lethality in homozygous

476 *Lrp2* mice due to holoprosencephaly, mimicking loss of Shh function. In contrast, a single point mutation
477 causing a premature stop codon after amino acid 2721 allows for significantly greater survival and leads
478 to eye enlargement and myopia (74–77). Prematurely terminating Lrp2 before the transmembrane
479 domain may produce exclusively the soluble extracellular domain, restricting Lrp2 activity to a ligand
480 trap function. Specifically engineered mutant alleles for Lrp2 should help illuminate the multi-modal
481 activities of Lrp2.

482 Importantly, we show that transcriptional upregulation of ECM components in the eye is one
483 outcome of *lrp2* inactivity, which directly suggests a mechanism for excessive eye growth and refractive
484 error to occur. Overall, our work along with that of others supports the concept that Lrp2 is a
485 homeostatic node that buffers and integrates multiple pathways to precisely control initial eye growth
486 and emmetropization. In its absence, subtle and sustained alterations in signaling impact eye size and
487 refraction and cause severe myopia.

Materials and Methods

Fish maintenance

Zebrafish (*Danio rerio*) were maintained at 28.5°C on an Aquatic Habitats recirculating filtered water system (Aquatic Habitats, Apopka, FL) in reverse-osmosis purified water supplemented with Instant Ocean salts (60 mg/l) on a 14 h light: 10 h dark lighting cycle and fed a standard diet (78). All animal husbandry and experiments were approved and conducted in accordance with the guidelines set forth by the Institutional Animal Care and Use Committee of the Medical College of Wisconsin.

Transgenesis

DNA constructs for transgenesis were generated by PCR amplifying genes or domains of interest from adult eye cDNA (*nog3* CDS, *grem2* CDS, *bmp4* CDS, full-length and domains of *lrp2*) or gDNA (*rpe65a* promoter) before using the Invitrogen Gateway system (Thermo Fisher Scientific, Waltham, MA) to generate entry clones. The Gateway system was further used to assemble promoter: gene-tag constructs using backbone vectors containing Tol2-inverted repeats flanking the transgene constructs to facilitate transgenic insertion into the zebrafish genome (79,80). Plasmid and primer sequences are available on request.

Spectral domain-optical coherence tomography (SD-OCT)

Zebrafish eyes were imaged using a Bioptigen Envisu R2200 SD-OCT imaging system with a 12 mm telecentric lens (Bioptigen, Morrisville, NC) essentially as described (46). To ensure uniform measuring of eyes, the iris edges were aligned in both dorsal-ventral and nasal-temporal planes before acquisition. Ocular dimensions were measured using the built-in manual caliper tool in the InVivoVue software platform with an applied refractive index constant of 1.30.

RNA extraction and RNAseq

lrp2$^{-/-}$ and wild-type zebrafish eyes were dissected at 1 mpf to give retinal, RPE and sclera/choroid samples. Each sample contained tissues from 10 – 20 eyes and was repeated in triplicate. RNA extracted from these samples was assayed for tissue specificity using retinal-, RPE- or sclera/choroid-specific marker genes by qPCR, before analyzing by RNAseq. RNA was processed for sequencing by BGI Americas (Cambridge, MA), using an Illumina HiSeqTM 2000 instrument, and Bowtie2 used to align to the current zebrafish genome (GRCz10 (GCA_000002035.3)).

Direct link to deposited data

The datasets supporting this article are available in the NCBI Gene Expression Omnibus (GEO) archive. Accession number for the data is GSE97125. Link to the data: https://www.ncbi.nlm.nih.gov/geo/query/acc.cgi?acc=GSE97125.

Gene set enrichment analysis (GSEA)

RNAseq datasets were analyzed for enrichment of genes associated with transcript signatures defined by overexpression of zebrafish Bmp4 and Shha. Briefly, datasets and signature gene lists were entered into the stand-alone GSEA tool (48,49). Resulting sets of enriched genes were tabulated using standard output criteria (enrichment score (ES), normalized enrichment score (NES), nominal p-value, false discovery rate q-value, family-wise error rate).

HEK293T cell culture and immunoprecipitation

Zebrafish Lrp2 LDLA domains 1 through 4 were individually placed under the control of a CMV promoter and tagged at their C-terminus with a 15 amino acid S•tag epitope, which can be immobilized using S•protein conjugated to agarose beads. The native Lrp2 signal peptide was placed upstream of

each LDLA domain to facilitate proper protein export. Zebrafish Bmp4 sequence was placed downstream of a CMV promoter, and an internal eGFP tag was placed after the furin cleavage sites so that when translated mature Bmp4 could be detected after removal of the prodomain (81). Plasmids *CMV:eGFP-bmp4* and *CMV:lrp2 (signal peptide-LDLAx)-S•tag* (where x represents one of the LDLA domains 1 – 4) were transfected into HEK293T cells for 24 hours. Proteins were extracted from pelleted cells using a gentle RIPA buffer, and incubated with S-protein agarose (EMD Millipore, Temecula, CA) before washing and eluting from agarose by boiling in reducing protein loading dye. Proteins were separated on Bio-Rad Any kD gradient SDS-PAGE gels before transferring to Immobilon-F PVDF membranes. Western blots were probed using anti-eGFP antibody JL-8 (Clontech, Mountain View, CA) and developed using the LI-COR Odyssey buffer and imaging system (LI-COR, Lincoln, NE).

Similarly, HEK293T cells were transfected with *pTol2-CMV:SP6-seGFP-lrp2 ECD-ICD-mCherry* plasmid DNA and cultured for 24 hours before adding inhibitors or activators of sheddases. These compounds were incubated with the cells for 24 hours before conditioned medium was collected. Conditioned medium was applied to GFP-Trap®_A agarose (Chromotek, Hauppauge, NY) for 2 hours before washing the agarose and eluting bound protein by boiling in reducing protein loading dye. Western blotting was carried out as above. Where appropriate, Western blot bands were quantified using ImageJ (Rasband, W.S., ImageJ, U. S. National Institutes of Health, MD).

Zebrafish in vivo Bmp reporter assay

BACE inhibitor compounds or DMSO as control were bath-applied to transgenic *BRE:d2GFP* zebrafish for 24 hours before imaging fluorescence in the eye using a Nikon Eclipse E600FN confocal fluorescent microscope (Nikon, Tokyo, Japan). Fluorescent intensity was measured in ImageJ by outlining the region of interest and measuring the integrated density for fluorescence, correcting for

559 background fluorescence (82). Double transgenic *BRE:d2GFP/ rpe65a:mCherry-CAAX* or *BRE:dmKO2*
560 zebrafish were imaged at 5 dpf to identify the GFP-positive tissue in the larval eye.
561
562 **Statistical analyses**
563 Eye measurements were processed using Microsoft Excel (Microsoft, Redmond, WA) and
564 graphed using GraphPad Prism (GraphPad, La Jolla, CA). Standard deviation (SD) and analysis of variance
565 (ANOVA) with post-test analyses were calculated using GraphPad Prism. Sample sizes were not
566 calculated in advance, but post hoc calculations showed that most experiments exceeded a statistical
567 power of 95% for alpha = 0.05. Post hoc sample sizes were calculated for axial length, axial length: body
568 axis, and axial length: lens diameter metrics, to detect an outcome of 10% change relative to wild-type
569 at 2 mpf and 3 mpf. An exception was 3 mpf wild-type axial length: lens diameter, where a 20% size
570 change could be detected with significance using the numbers of animals tested. *lrp2*$^{-/-}$ mutant eye
571 metrics usually changed by more than 10% of the wild-type metric under consideration.
572
573 **Acknowledgements**
574 The authors thank Michael Cliff and William Hudzinski for zebrafish husbandry. We are also
575 grateful to Amy Ludwig-Kubinkski, Jason Bader and Amira Pavlovich for assistance and advice on cell
576 culture and Western blotting. Finally, we are indebted to Dr. Joe Besharse for critical feedback and
577 suggestions. This work was supported by National Institutes of Health/National Eye Institute R01
578 research grant EY016060 (BAL) as well as a Core Grant for Vision Research (P30 EY001931).
579
580
581

582 **Competing Interests**

583 The authors have no competing interests of any kind to disclose.

584

585

586

References

1. Storm T, Heegaard S, Christensen EI, Nielsen R. Megalin–deficiency causes high myopia, retinal pigment epithelium-macromelanosomes and abnormal development of the ciliary body in mice. Cell Tissue Res. 2014;358(1):99–107.

2. Assémat E, Châtelet F, Chandellier J, Commo F, Cases O, Verroust P, et al. Overlapping expression patterns of the multiligand endocytic receptors cubilin and megalin in the CNS, sensory organs and developing epithelia of the rodent embryo. Gene Expr Patterns. 2005 Dec;6(1):69–78.

3. Zheng G, Bachinsky DR, Stamenkovic I, Strickland DK, Brown D, Andres G, et al. Organ distribution in rats of two members of the low-density lipoprotein receptor gene family, gp330 and LRP/alpha 2MR, and the receptor-associated protein (RAP). J Histochem Cytochem Off J Histochem Soc. 1994 Apr;42(4):531–42.

4. Christensen EI, Raciti D, Reggiani L, Verroust PJ, Brändli AW. Gene expression analysis defines the proximal tubule as the compartment for endocytic receptor-mediated uptake in the Xenopus pronephric kidney. Pflüg Arch Eur J Physiol. 2008 Sep;456(6):1163–76.

5. Kerjaschki D, Noronha-Blob L, Sacktor B, Farquhar MG. Microdomains of distinctive glycoprotein composition in the kidney proximal tubule brush border. J Cell Biol. 1984 Apr;98(4):1505–13.

6. Kantarci S, Al-Gazali L, Hill RS, Donnai D, Black GCM, Bieth E, et al. Mutations in LRP2, which encodes the multiligand receptor megalin, cause Donnai-Barrow and facio-oculo-acoustico-renal syndromes. Nat Genet. 2007 Aug;39(8):957–9.

7. Donnai D, Barrow M. Diaphragmatic hernia, exomphalos, absent corpus callosum, hypertelorism, myopia, and sensorineural deafness: a newly recognized autosomal recessive disorder? Am J Med Genet. 1993 Oct 1;47(5):679–82.

8. Pober BR, Longoni M, Noonan KM. A review of Donnai-Barrow and facio-oculo-acoustico-renal (DB/FOAR) syndrome: clinical features and differential diagnosis. Birt Defects Res A Clin Mol Teratol. 2009 Jan;85(1):76–81.

9. Christ A, Christa A, Klippert J, Eule JC, Bachmann S, Wallace VA, et al. LRP2 Acts as SHH Clearance Receptor to Protect the Retinal Margin from Mitogenic Stimuli. Dev Cell. 2015 Oct 12;35(1):36–48.

10. Christ A, Christa A, Kur E, Lioubinski O, Bachmann S, Willnow TE, et al. LRP2 is an auxiliary SHH receptor required to condition the forebrain ventral midline for inductive signals. Dev Cell. 2012 Feb 14;22(2):268–78.

11. Spoelgen R, Hammes A, Anzenberger U, Zechner D, Andersen OM, Jerchow B, et al. LRP2/megalin is required for patterning of the ventral telencephalon. Development. 2005;132(2):405–14.

12. Zou Z, Chung B, Nguyen T, Mentone S, Thomson B, Biemesderfer D. Linking Receptor-mediated Endocytosis and Cell Signaling: evidence for regulated intramembrane proteolysis of megalin in proximal tubule. J Biol Chem. 2004 Aug 13;279(33):34302–10.

13. Li Y, Cong R, Biemesderfer D. The COOH terminus of megalin regulates gene expression in opossum kidney proximal tubule cells. Am J Physiol - Cell Physiol. 2008 Aug 1;295(2):C529–37.

14. Christ A, Terryn S, Schmidt V, Christensen EI, Huska MR, Andrade-Navarro MA, et al. The soluble intracellular domain of megalin does not affect renal proximal tubular function in vivo. Kidney Int. 2010 Sep;78(5):473–7.

15. Ishida T, Hatae T, Nishi N, Araki N. Soluble megalin is accumulated in the lumen of the rat endolymphatic sac. Cell Struct Funct. 2006;31(2):77–85.

16. Bachinsky DR, Zheng G, Niles JL, McLaughlin M, Abbate M, Andres G, et al. Detection of two forms of GP330. Their role in Heymann nephritis. Am J Pathol. 1993 Aug;143(2):598–611.

17. Orlando RA, Farquhar MG. Identification of a cell line that expresses a cell surface and a soluble form of the gp330/receptor-associated protein (RAP) Heymann nephritis antigenic complex. Proc Natl Acad Sci U S A. 1993 May 1;90(9):4082–6.

18. Jung FF, Bachinsky DR, Tang SS, Zheng G, Diamant D, Haveran L, et al. Immortalized rat proximal tubule cells produce membrane bound and soluble megalin. Kidney Int. 1998 Feb;53(2):358–66.

19. Norden AGW, Lapsley M, Igarashi T, Kelleher CL, Lee PJ, Matsuyama T, et al. Urinary megalin deficiency implicates abnormal tubular endocytic function in Fanconi syndrome. J Am Soc Nephrol JASN. 2002 Jan;13(1):125–33.

20. Pizzarello L, Abiose A, Ffytche T, Duerksen R, Thulasiraj R, Taylor H, et al. VISION 2020: The Right to Sight: a global initiative to eliminate avoidable blindness. Arch Ophthalmol. 2004 Apr;122(4):615–20.

21. Resnikoff S, Pascolini D, Mariotti SP, Pokharel GP. Global magnitude of visual impairment caused by uncorrected refractive errors in 2004. Bull World Health Organ. 2008 Jan;86(1):63–70.

22. Iwase A, Araie M, Tomidokoro A, Yamamoto T, Shimizu H, Kitazawa Y, et al. Prevalence and causes of low vision and blindness in a Japanese adult population: the Tajimi Study. Ophthalmology. 2006 Aug;113(8):1354–62.

23. Wu L, Sun X, Zhou X, Weng C. Causes and 3-year-incidence of blindness in Jing-An District, Shanghai, China 2001-2009. BMC Ophthalmol. 2011;11:10.

24. Vitale S, Ellwein L, Cotch MF, Ferris FL, Sperduto R. Prevalence of refractive error in the United States, 1999–2004. Arch Ophthalmol. 2008 Aug;126(8):1111–9.

25. Kiefer AK, Tung JY, Do CB, Hinds DA, Mountain JL, Francke U, et al. Genome-wide analysis points to roles for extracellular matrix remodeling, the visual cycle, and neuronal development in myopia. PLoS Genet. 2013;9(2):e1003299.

26. Verhoeven VJM, Hysi PG, Wojciechowski R, Fan Q, Guggenheim JA, Höhn R, et al. Genome-wide meta-analyses of multiancestry cohorts identify multiple new susceptibility loci for refractive error and myopia. Nat Genet. 2013 May 29;45(6):712.

27. Jones LA, Sinnott LT, Mutti DO, Mitchell GL, Moeschberger ML, Zadnik K. Parental history of myopia, sports and outdoor activities, and future myopia. Invest Ophthalmol Vis Sci. 2007 Aug;48(8):3524–32.

28. Rose KA, Morgan IG, Ip J, Kifley A, Huynh S, Smith W, et al. Outdoor activity reduces the prevalence of myopia in children. Ophthalmology. 2008 Aug;115(8):1279–85.

29. Wallman J, Winawer J. Homeostasis of eye growth and the question of myopia. Neuron. 2004 Aug 19;43(4):447–68.

30. Bakrania P, Efthymiou M, Klein JC, Salt A, Bunyan DJ, Wyatt A, et al. Mutations in BMP4 cause eye, brain, and digit developmental anomalies: overlap between the BMP4 and hedgehog signaling pathways. Am J Hum Genet. 2008 Feb;82(2):304–19.

31. Reis LM, Tyler RC, Schilter KF, Abdul-Rahman O, Innis JW, Kozel BA, et al. BMP4 loss-of-function mutations in developmental eye disorders including SHORT syndrome. Hum Genet. 2011 Oct;130(4):495–504.

32. McGlinn AM, Baldwin DA, Tobias JW, Budak MT, Khurana TS, Stone RA. Form-deprivation myopia in chick induces limited changes in retinal gene expression. Invest Ophthalmol Vis Sci. 2007 Aug;48(8):3430–6.

33. Wang Q, Xue M-L, Zhao G-Q, Liu M-G, Ma Y-N, Ma Y. Form-deprivation myopia induces decreased expression of bone morphogenetic protein-2, 5 in guinea pig sclera. Int J Ophthalmol. 2015;8(1):39–45.

34. Wang Q, Zhao G, Xing S, Zhang L, Yang X. Role of bone morphogenetic proteins in form-deprivation myopia sclera. Mol Vis. 2011;17:647–57.

35. Li H, Cui D, Zhao F, Huo L, Hu J, Zeng J. BMP-2 Is Involved in Scleral Remodeling in Myopia Development. PLoS ONE [Internet]. 2015 May 12 [cited 2015 Jun 2];10(5). Available from: http://www.ncbi.nlm.nih.gov/pmc/articles/PMC4429026/

36. Zhang Y, Liu Y, Wildsoet CF. Bidirectional, optical sign-dependent regulation of BMP2 gene expression in chick retinal pigment epithelium. Invest Ophthalmol Vis Sci. 2012;53(10):6072–80.

37. Zhang Y, Liu Y, Ho C, Wildsoet CF. Effects of imposed defocus of opposite sign on temporal gene expression patterns of BMP4 and BMP7 in chick RPE. Exp Eye Res. 2013 Apr;109:98–106.

38. Potti TA, Petty EM, Lesperance MM. A comprehensive review of reported heritable noggin-associated syndromes and proposed clinical utility of one broadly inclusive diagnostic term: NOG-related-symphalangism spectrum disorder (NOG-SSD). Hum Mutat. 2011 Aug 1;32(8):877–86.

39. Brown DJ, Kim TB, Petty EM, Downs CA, Martin DM, Strouse PJ, et al. Autosomal dominant stapes ankylosis with broad thumbs and toes, hyperopia, and skeletal anomalies is caused by heterozygous nonsense and frameshift mutations in NOG, the gene encoding noggin. Am J Hum Genet. 2002 Sep;71(3):618–24.

40. Milunsky J, Suntra C, MacDonald CB. Congenital stapes ankylosis, broad thumbs, and hyperopia: report of a family and refinement of a syndrome. Am J Med Genet. 1999 Feb 19;82(5):404–8.

41. Sieber C, Kopf J, Hiepen C, Knaus P. Recent advances in BMP receptor signaling. Cytokine Growth Factor Rev. 2009 Dec;20(5–6):343–55.

42. Brazil DP, Church RH, Surae S, Godson C, Martin F. BMP signalling: agony and antagony in the family. Trends Cell Biol. 2015 May 1;25(5):249–64.

43. Veth KN, Willer JR, Collery RF, Gray MP, Willer GB, Wagner DS, et al. Mutations in zebrafish lrp2 result in adult-onset ocular pathogenesis that models myopia and other risk factors for glaucoma. PLoS Genet. 2011 Feb;7(2):e1001310.

44. Sherpa T, Hunter SS, Frey RA, Robison BD, Stenkamp DL. Retinal proliferation response in the buphthalmic zebrafish, bugeye. Exp Eye Res. 2011 Oct;93(4):424–36.

45. Stujenske JM, Dowling JE, Emran F. The Bugeye Mutant Zebrafish Exhibits Visual Deficits that Arise with the Onset of an Enlarged Eye Phenotype. Invest Ophthalmol Vis Sci. 2011;52(7):4200–7.

46. Collery RF, Veth KN, Dubis AM, Carroll J, Link BA. Rapid, Accurate, and Non-Invasive Measurement of Zebrafish Axial Length and Other Eye Dimensions Using SD-OCT Allows Longitudinal Analysis of Myopia and Emmetropization. PloS One. 2014;9(10):e110699.

47. Shen M-C, Ozacar AT, Osgood M, Boeras C, Pink J, Thomas J, et al. Heat-shock-mediated conditional regulation of hedgehog/gli signaling in zebrafish. Dev Dyn Off Publ Am Assoc Anat. 2013 May;242(5):539–49.

48. Mootha VK, Lindgren CM, Eriksson K-F, Subramanian A, Sihag S, Lehar J, et al. PGC-1α-responsive genes involved in oxidative phosphorylation are coordinately downregulated in human diabetes. Nat Genet. 2003 Jul;34(3):267–73.

49. Subramanian A, Tamayo P, Mootha VK, Mukherjee S, Ebert BL, Gillette MA, et al. Gene set enrichment analysis: a knowledge-based approach for interpreting genome-wide expression profiles. Proc Natl Acad Sci U S A. 2005 Oct 25;102(43):15545–50.

50. Boulanger A, Liu S, Henningsgaard AA, Yu S, Redmond TM. The Upstream Region of the Rpe65 Gene Confers Retinal Pigment Epithelium-specific Expression in Vivo and in Vitro and Contains Critical Octamer and E-box Binding Sites. J Biol Chem. 2000 Oct 6;275(40):31274–82.

51. Kwan KM, Otsuna H, Kidokoro H, Carney KR, Saijoh Y, Chien C-B. A complex choreography of cell movements shapes the vertebrate eye. Dev Camb Engl. 2012 Jan;139(2):359–72.

52. Collery RF, Veth KN, Dubis AM, Carroll J, Link BA. Rapid, accurate, and non-invasive measurement of zebrafish axial length and other eye dimensions using SD-OCT allows longitudinal analysis of myopia and emmetropization. PLoS ONE. in press;

53. Chocron S, Verhoeven MC, Rentzsch F, Hammerschmidt M, Bakkers J. Zebrafish Bmp4 regulates left–right asymmetry at two distinct developmental time points. Dev Biol. 2007 May 15;305(2):577–88.

54. Collery RF, Link BA. Dynamic smad-mediated BMP signaling revealed through transgenic zebrafish. Dev Dyn Off Publ Am Assoc Anat. 2011 Mar;240(3):712–22.

55. Higdon CW, Mitra RD, Johnson SL. Gene expression analysis of zebrafish melanocytes, iridophores, and retinal pigmented epithelium reveals indicators of biological function and developmental origin. PloS One. 2013;8(7):e67801.

56. Spoelgen R, Hammes A, Anzenberger U, Zechner D, Andersen OM, Jerchow B, et al. LRP2/megalin is required for patterning of the ventral telencephalon. Dev Camb Engl. 2005 Jan;132(2):405–14.

57. Collery RF, Link BA. Dynamic smad-mediated BMP signaling revealed through transgenic zebrafish. Dev Dyn. 2011;240(3):712–22.

58. Mutti DO, Cooper ME, O'Brien S, Jones LA, Marazita ML, Murray JC, et al. Candidate gene and locus analysis of myopia. Mol Vis. 2007 Jun 28;13:1012–9.

59. Metlapally R, Li Y-J, Tran-Viet K-N, Abbott D, Czaja GR, Malecaze F, et al. COL1A1 and COL2A1 genes and myopia susceptibility: evidence of association and suggestive linkage to the COL2A1 locus. Invest Ophthalmol Vis Sci. 2009 Sep;50(9):4080–6.

60. Lin H-J, Wan L, Tsai Y, Liu S-C, Chen W-C, Tsai S-W, et al. Sclera-related gene polymorphisms in high myopia. Mol Vis. 2009 Aug 20;15:1655–63.

61. Zha Y, Leung KH, Lo KK, Fung WY, Ng PW, Shi M, et al. TGFB1 as a susceptibility gene for high myopia: a replication study with new findings. Arch Ophthalmol Chic Ill 1960. 2009 Apr;127(4):541–8.

62. Hall NF, Gale CR, Ye S, Martyn CN. Myopia and polymorphisms in genes for matrix metalloproteinases. Invest Ophthalmol Vis Sci. 2009 Jun;50(6):2632–6.

63. Wojciechowski R, Bailey-Wilson JE, Stambolian D. Association of matrix metalloproteinase gene polymorphisms with refractive error in Amish and Ashkenazi families. Invest Ophthalmol Vis Sci. 2010 Oct;51(10):4989–95.

64. Chen ZT-Y, Wang I-J, Shih Y-F, Lin LL-K. The association of haplotype at the lumican gene with high myopia susceptibility in Taiwanese patients. Ophthalmology. 2009 Oct;116(10):1920–7.

65. Hernandez H, Millar JC, Curry SM, Clark AF, McDowell CM. BMP and Activin Membrane Bound Inhibitor Regulates the Extracellular Matrix in the Trabecular Meshwork. Invest Ophthalmol Vis Sci. 2018 Apr 1;59(5):2154–66.

66. Wordinger RJ, Fleenor DL, Hellberg PE, Pang I-H, Tovar TO, Zode GS, et al. Effects of TGF-beta2, BMP-4, and gremlin in the trabecular meshwork: implications for glaucoma. Invest Ophthalmol Vis Sci. 2007 Mar;48(3):1191–200.

67. Wordinger RJ, Sharma T, Clark AF. The role of TGF-β2 and bone morphogenetic proteins in the trabecular meshwork and glaucoma. J Ocul Pharmacol Ther Off J Assoc Ocul Pharmacol Ther. 2014 Apr;30(2–3):154–62.

68. Zode GS, Clark AF, Wordinger RJ. Bone morphogenetic protein 4 inhibits TGF-beta2 stimulation of extracellular matrix proteins in optic nerve head cells: role of gremlin in ECM modulation. Glia. 2009 May;57(7):755–66.

69. Mody AA, Wordinger RJ, Clark AF. Role of ID Proteins in BMP4 Inhibition of Profibrotic Effects of TGF-β2 in Human TM Cells. Invest Ophthalmol Vis Sci. 2017 01;58(2):849–59.

70. Cases O, Joseph A, Obry A, Santin MD, Ben-Yacoub S, Pâques M, et al. Foxg1-Cre Mediated Lrp2 Inactivation in the Developing Mouse Neural Retina, Ciliary and Retinal Pigment Epithelia Models Congenital High Myopia. PLoS ONE [Internet]. 2015 Jun 24 [cited 2016 Jun 13];10(6). Available from: http://www.ncbi.nlm.nih.gov/pmc/articles/PMC4480972/

71. Pi X, Schmitt CE, Xie L, Portbury AL, Wu Y, Lockyer P, et al. LRP1-dependent endocytic mechanism governs the signaling output of the bmp system in endothelial cells and in angiogenesis. Circ Res. 2012 Aug 17;111(5):564–74.

72. Fielden MR, Werner J, Jamison JA, Coppi A, Hickman D, Dunn RT, et al. Retinal Toxicity Induced by a Novel β-secretase Inhibitor in the Sprague-Dawley Rat. Toxicol Pathol. 2014 Oct 31;0192623314553804.

73. Cai J, Qi X, Kociok N, Skosyrski S, Emilio A, Ruan Q, et al. β-Secretase (BACE1) inhibition causes retinal pathology by vascular dysregulation and accumulation of age pigment. EMBO Mol Med. 2012 Sep;4(9):980–91.

74. Willnow TE, Hilpert J, Armstrong SA, Rohlmann A, Hammer RE, Burns DK, et al. Defective forebrain development in mice lacking gp330/megalin. Proc Natl Acad Sci. 1996 Aug 6;93(16):8460–4.

75. Baardman ME, Zwier MV, Wisse LJ, Gittenberger-de Groot AC, Kerstjens-Frederikse WS, Hofstra RMW, et al. Common arterial trunk and ventricular non-compaction in Lrp2 knockout mice indicate a crucial role of LRP2 in cardiac development. Dis Model Mech. 2016 Apr 1;9(4):413–25.

76. Zarbalis K, May SR, Shen Y, Ekker M, Rubenstein JLR, Peterson AS. A focused and efficient genetic screening strategy in the mouse: identification of mutations that disrupt cortical development. PLoS Biol. 2004 Aug;2(8):E219.

77. Gajera CR, Emich H, Lioubinski O, Christ A, Beckervordersandforth-Bonk R, Yoshikawa K, et al. LRP2 in ependymal cells regulates BMP signaling in the adult neurogenic niche. J Cell Sci. 2010 Jun 1;123(11):1922–30.

78. Westerfield M. ZEBRAFISH BOOK, 5th Edition; A guide for the laboratory use of zebrafish (Danio rerio). Eugene, Oregon: University of Oregon Press; 2007.

79. Kawakami K, Shima A, Kawakami N. Identification of a functional transposase of the Tol2 element, an Ac-like element from the Japanese medaka fish, and its transposition in the zebrafish germ lineage. Proc Natl Acad Sci U A. 2000;97(21):11403–8.

80. Kwan KM, Fujimoto E, Grabher C, Mangum BD, Hardy ME, Campbell DS, et al. The Tol2kit: a multisite gateway-based construction kit for Tol2 transposon transgenesis constructs. Dev Dyn. 2007;236(11):3088–99.

800 81. Entchev EV, Schwabedissen A, Gonzalez-Gaitan M. Gradient formation of the TGF-beta homolog
801 Dpp. Cell. 2000 Dec 8;103(6):981–91.

802 82. Burgess A, Vigneron S, Brioudes E, Labbé J-C, Lorca T, Castro A. Loss of human Greatwall results in
803 G2 arrest and multiple mitotic defects due to deregulation of the cyclin B-Cdc2/PP2A balance. Proc
804 Natl Acad Sci U S A. 2010 Jul 13;107(28):12564–9.

805

806

807 **Figure Legend**

808 **Figure 1. The zebrafish *rpe65a* promoter drives transgene expression in the developing and adult**
809 **RPE.** A - D. the *rpe65a* promoter drives expression in the 5 dpf RPE (A,B, cryosection; C, D, en face in
810 vivo). E - H. Strong eGFP expression is seen in the 3 mpf adult retina but not the CMZ. I –L. RPE
811 expression (green) driven by the *rpe65a* promoter contrasts with red-green cone-specific zpr-1 antibody
812 staining (magenta). M – P. Similarly, eGFP in RPE cells contrast with rod-specific zpr-3 antibody staining
813 (magenta). Scale bars: A, B, E – P = 50 µm; C, D = 10 µM. RPE, retinal pigment epithelium; PhR,
814 photoreceptor; ONL, outer nuclear layer; INL, inner nuclear layer; GCL, ganglion cell layer; CMZ, ciliary
815 marginal zone.

816

817 **Figure 2. *rpe65a*-driven Lrp2 partially rescues the myopic *lrp2/bugeye* phenotype in adult**
818 **zebrafish.** A. Eye axial length: lens diameter ratio is reduced in *lrp2*$^{-/-}$ expressing RPE-derived Lrp2 at 3
819 mpf (0.09143 vs 0.1130; p=0.0001; Kruskal-Wallis test). However, *lrp2*$^{-/-}$ *rpe65a>lrp2-HA* eyes still have a
820 significantly greater eye axial length: lens diameter ratio than wild-type controls (0.088 vs 0.1130;
821 p<0.0001; Kruskal-Wallis test). B. Similarly, the relative refractive error is lessened in *lrp2*$^{-/-}$ eyes
822 expressing RPE-derived Lrp2 at 3 mpf (-0.6013 vs -1.066; p<0.0001; Kruskal-Wallis test). This rescue is
823 partial and does not restore myopic *lrp2*$^{-/-}$ eyes to emmetropia (0.048 vs -1.066; p<0.0001; Kruskal-
824 Wallis test). This experiment was performed twice for validation with similar results.

825

826 **Figure 3. *rpe65a*-driven Noggin3 expression causes myopia in wild-type zebrafish and exacerbates**
827 **myopia in *lrp2/bugeye* adults, while *rpe65a*-driven Gremlin2 expression exacerbates myopia in *lrp2*$^{-/-}$**
828 **but not wild-type.** A. RPE-derived Nog3 causes an increase in axial length: lens diameter ratio in both
829 *lrp2*$^{-/-}$ and wild-type zebrafish at 2 mpf (*lrp2*$^{-/-}$: 2.14 vs 1.82; p=0.0037; Mann-Whitney test. *lrp2*$^{+/-}$: 1.76
830 vs 1.66; p=0.0019; Mann-Whitney test. n= 5 for *lrp2*$^{+/-}$ *rpe65a>nog*; n= 7 for *lrp2*$^{-/-}$ *rpe65a>nog*; n = 12

for *lrp2*$^{+/-}$ *rpe65a:Gal4*; n = 16 for *lrp2*$^{-/-}$ *rpe65a:Gal4*). B. RPE-derived Nog3 expression worsens the degree of relative refractive error in both *lrp2*$^{-/-}$ and wild-type zebrafish at 2 mpf (*lrp2*$^{-/-}$: 0.262 vs 0.049; p=0.0299; Mann-Whitney test. *lrp2*$^{+/-}$: -0.029 vs 0.044; p=0.0019; Mann-Whitney test.). C. RPE-derived Grem2 causes an increase in axial length: lens diameter ratio in *lrp2*$^{-/-}$ zebrafish at 2 mpf, but not in wild-type (*lrp2*$^{-/-}$: 1.87 vs 1.78; p=0.0054; Mann-Whitney test. n was greater than 24 for each genotype, except for *lrp2*$^{-/-}$ *rpe65a:Gal4*, where n = 16.). D. RPE-derived Grem2 expression worsens the degree of relative refractive error in *lrp2*$^{-/-}$ zebrafish at 2 mpf, but not wild-type (*lrp2*$^{-/-}$: -0.143 vs -0.076; p=0.0051; Mann-Whitney test.).

Figure 4. The first LDLA domain of Lrp2 binds Bmp4 *in vivo*. A. Schematic showing the structure of Lrp2 with four LDLA domains that bind cognate ligands. B – E. Expression of individual LDLA domains 1 – 4 with eGFP-Bmp4 shows that immobilized LDLA1-S•tag can bind Bmp4, but that the other LDLA domains cannot.

Figure 5. *rpe65a*-driven soluble Lrp2 (LDLA1) exacerbates myopia in *lrp2/bugeye* adults. A. RPE-derived Lrp2 (LDLA1) causes an increase in axial length: lens diameter ratio in *lrp2*$^{-/-}$ zebrafish at 2 mpf, but not in wild-type (*lrp2*$^{-/-}$: 1.98 vs 1.78; p<0.0001; Mann-Whitney test. n = greater than 20 for each genotype.). B. RPE-derived Lrp2 (LDLA1) expression worsens the degree of relative refractive error in *lrp2*$^{-/-}$ zebrafish at 2 mpf, but not wild-type(*lrp2*$^{-/-}$: -0.197 vs -0.063; p<0.0001; Mann-Whitney test.).

Figure 6. Lrp2 is cleaved extracellularly by a BACE family member to release a soluble form. A. Schematic showing tagging of a 432 amino acid region of Lrp2 with secreted eGFP at the N-terminus and mCherry at the C-terminus to monitor extracellular cleavage, referred to as seGFP-Lrp2 (ECD/ICD)-mCherry. B - D. HEK293T cells transfected with seGFP-Lrp2 (ECD/ICD)-mCherry were treated 24 hours

after transfection with compounds and grown for another 24 hours before harvesting conditioned medium. eGFP-tagged domains cleaved from seGFP-Lrp2 (ECD/ICD)-mCherry were immobilized using Chromotek GFP-binding agarose before Western blotting and detection with JL-8 (anti-GFP antibody). E. When soluble eGFP-species levels from post-drug treatments were normalized to pre-treatment levels from the same culture plates, LY2811376-treatment appeared to reduce extracellular cleavage of seGFP-Lrp2 (ECD/ICD)-mCherry. Pixel intensity is expressed in arbitrary units based on ImageJ measurements of Western blot band densities.

Figure 7. Inhibition of BACE enzyme activity in zebrafish increases Bmp signaling in the choroid/sclera of the eye. Incubation of 4-5 dpf *BRE:d2GFP* larvae with LY2811376 or BACE inhibitor II caused increased levels of Bmp signaling in the choroid/sclera of the eye compared to DMSO-treated control siblings. n = 10 for LY2811376 treatment; n= 9 for BACE inhibitor II treatment; n = 9 for DMSO control treatment.

Figure 8. Expression of soluble, but not membrane-bound, Lrp2 LDLA1 from RPE downregulates Bmp signaling in the choroid/sclera. A, B *rpe65a:Lrp2 LDLA1-eGFP* or *rpe65a:Lrp2 LDLA1-ICD-eGFP* plasmids were injected into BRE:dmKO2 reporter zebrafish and eye fluorescence measured at 4 dpf. C. Sclera/choroidal expression levels were unchanged from uninjected controls with Lrp2 LDLA1-ICD-eGFP (uninjected, 301 arbitrary units ± 173; Lrp2 LDLA1-ICD-eGFP, 320 arbitrary units ± 109), while Lrp2 LDLA1-eGFP expression led to significant reduction of Bmp activity (153 arbitrary units ± 73). Fluorescence levels were compared using one-way ANOVA with Tukey's post-hoc test.

Figure 9. Expression of ECM components is upregulated in *lrp2*$^{-/-}$ eyes. GSEA analysis using an ECM-receptor KEGG pathway converted to zebrafish orthologs to query 1 mpf eyes show enrichment of ECM

879 gene expression with a normalized enrichment score = 1.897 for *lrp2*$^{-/-}$ eyes (nominal p value = 0.002,
880 FDR q = 0.002, FWER p = 0.001).
881
882
883 **Figure 10. Model – Modulation of Lrp2-mediated Bmp4 signaling by extracellular cleavage allows**
884 **fine-tuning of ligand levels between the RPE and sclera/choroid.** Lrp2 may facilitate Bmp4 signaling
885 while the extracellular region of Lrp2 is tethered by its transmembrane domain. Extracellular cleavage of
886 Lrp2 by member of the BACE protein family converts the soluble domain to a decoy receptor that no
887 longer facilitates signaling. Absence of membrane-bound Lrp2 leads to reduced Bmp signaling which is
888 associated with excessive eye growth. When *lrp2*$^{-/-}$ eyes with already reduced Bmp signaling express
889 transgenic Lrp2 LDLA1 from the RPE, some Bmp ligands are bound by this decoy, further reducing Bmp
890 signaling and increasing excessive eye growth even more.
891
892 **Table 1. Gene set enrichment analysis of wild-type and *lrp2*$^{-/-}$ zebrafish eyes and dissected tissues**
893 **using Bmp4 and Shha pathway signature sets from this work.** GSEA analyses were conducted on
894 RNAseq datasets from whole eye and dissected eye tissues using custom BMP4 and Shha-specific
895 signatures. p-values lower than 0.05 were scored as +1, while p-values greater than 0.05 were scored as
896 0. The final scores were summed and used to rank significance of each signaling pathway in each tissue.
897
898 **S1 Figure. qPCR with tissue-specific markers shows high levels of purity for dissected**
899 **sclera/choroid, RPE and retina.** Dissected sclera, RPE and retina were assayed for expression of genes
900 enriched in those tissues (*col1a1a*, *col12a1a*, sclera/choroid; *rpe65a*, *rlbp1b*, RPE; *gnat2*, *pde6c*, retina).
901 Enrichment levels for each tissue are shown as normalized $\Delta\Delta$Cq (A), or as percentages (B).
902

S1 Table. RNAseq datasets comparing wild-type and *lrp2*$^{-/-}$ zebrafish whole eyes, choroid/sclera, RPE and retina at 1 mpf, filtered for p<0.01, 50 RNAseq reads, and representation in all three sample replicates.

S2 Table. FPKM (Fragments Per Kilobase Million) gene transcript levels for 1 mpf wild-type and *lrp2*$^{-/-}$ zebrafish eyes and dissected eye tissues.

S3 Table. RNAseq datasets comparing wild-type and *lrp2*$^{-/-}$ zebrafish whole eyes, choroid/sclera, RPE and retina at 1 mpf, filtered for p<0.01, 50 fragments per kilobase of transcript per million mapped reads, and representation in all three sample replicates analyzed with Bmp4 and Shha signature pathway genes from this work.

S2 Figure. Bmp4 gene signatures used in this study. A, B. Genes up- or down-regulated in 5 dpf eyes from *hsp70l:eGFP-bmp4* transgenic larvae compared with non-transgenic sibling controls were filtered for representation in three independent samples, and used to define zebrafish Bmp4-UP and Bmp4-DOWN gene signatures. C, D. Gene lists of the signature genes identified in A and B.

S3 Figure. Shha gene signatures used in this study. A, B. Genes up- or down-regulated in 5 dpf eyes from *hsp70l:shha-eGFP* transgenic larvae compared with non-transgenic sibling controls were filtered for representation in two independent samples, and used to define zebrafish Shha-UP and Shha-DOWN gene signatures. C, D. Gene lists of the signature genes identified in A and B.

S4 Figure. Internal tagging of Bmp4 with eGFP allows *in vivo* tracking of the morphogen without loss of activity. A. Schematic of Bmp4 showing insertion of eGFP downstream of furin cleavage sites tagging

927 the mature ligand. B. Multiple cleavage forms of eGFP-Bmp4 can be seen on Western blots of larval
928 zebrafish extracts expressing eGFP-Bmp4 under the control of a heat-shock inducible promoter. The
929 bands likely correspond to full-length propeptide eGFP-Bmp4, mature cleaved eGFP-Bmp4, and
930 intermediates. C - F. eGFP-Bmp4 is secreted from cells in the developing embryos following expression.
931 G, H. Overexpression of eGFP-Bmp in the developing embryos causes a ventralized phenotype. I –T.
932 Overexpression of eGFP-Bmp4 in BRE-dmKO2 show perdurance of secreted Bmp4 24 hours after
933 transgenic expression.
934
935 **S5 Figure. *rpe65a*-driven eGFP-Bmp4 causes larval coloboma and severe eye disorganization in**
936 **adult zebrafish.** A, E. rpe65a-derived eGFP-Bmp4 causes larval phenotypes including coloboma. The
937 failure of the optic fissure to close properly is often accompanied by prognathia of the mandible. Most
938 larvae die, but some survive to adulthood, and show severe eye disorganization. F – L. Coloboma is seen
939 where the optic fissure remains open with the lens protruding. Staining with anti-cone arrestin 3
940 antibody, zpr-1, shows normally laminated cones in wild-type adults, but disorganization in plasmid-
941 injected adults, where photoreceptor rosetting is seen.
942
943 **S6 Figure. RNAseq shows enriched expression of Bmp ligands in the RPE and choroid/sclera.** Bmp
944 ligand family members, Bmp receptor family members and activin family members were assayed for
945 expression levels in whole eyes and dissected eye tissues.
946
947 **S7 Figure. Zebrafish Lrp2 contains putative consensus substrate sites for BACE enzyme cleavage.**
948 CLUSTAL alignments between zebrafish Lrp2 and published substrate sites of BACE show some
949 homology. Locations of putative cleavage sites are indicated on a schematic representation of Lrp2.
950

Tissue	Pathway	Bmp4	Bmp4	Shha	Shha	Nominal score	
Whole eye	**Direction of regulation**	**Up**	**Down**	**Up**	**Down**	**Bmp4**	**Shha**
Upregulated in class		*lrp2*	wild-type	wild-type	*lrp2*		
Enrichment Score (ES)		0.272	-0.343	-0.469	0.353		
Normalized Enrichment Score (NES)		1.183	-1.410	-1.887	1.415		
Nominal p-value		0.114	0.024	0.000	0.020		
FDR q-value		0.114	0.024	0.000	0.020		
FWER p-Value		0.087	0.008	0.000	0.014		
Score		0	+1	+1	+1	+1	+2

Tissue	Pathway	Bmp4	Bmp4	Shha	Shha
Sclera/choroid	**Direction of regulation**	**Up**	**Down**	**Up**	**Down**
Upregulated in class		*lrp2*	*lrp2*	wild-type	*lrp2*
Enrichment Score (ES)		0.263	0.457	-0.383	0.381
Normalized Enrichment Score (NES)		1.121	1.712	-1.680	1.489
Nominal p-value		0.221	0.002	0.010	0.011
FDR q-value		0.221	0.002	0.010	0.011
FWER p-Value		0.205	0.002	0.002	0.009
Score		0	+1	+1	+1	+1	+2

Tissue	Pathway	Bmp4	Bmp4	Shha	Shha
RPE	**Direction of regulation**	**Up**	**Down**	**Up**	**Down**
Upregulated in class		*lrp2*	wild-type	wild-type	*lrp2*
Enrichment Score (ES)		0.353	-0.327	-0.507	0.337
Normalized Enrichment Score (NES)		1.598	-1.408	-2.130	1.387
Nominal p-value		0.001	0.017	0.000	0.032
FDR q-value		0.001	0.017	0.000	0.032
FWER p-Value		0.001	0.005	0.000	0.024
Score		+1	+1	+1	+1	+2	+2

Tissue	Pathway	Bmp4	Bmp4	Shha	Shha
retina	**Direction of regulation**	**Up**	**Down**	**Up**	**Down**
Upregulated in class		wild-type	wild-type	wild-type	*lrp2*
Enrichment Score (ES)		-0.256	-0.241	-0.419	0.338
Normalized Enrichment Score (NES)		-1.181	-0.969	-1.607	1.425
Nominal p-value		0.074	0.499	0.012	0.017
FDR q-value		0.074	0.499	0.012	0.017
FWER p-Value		0.041	0.270	0.006	0.008
Score		+1	0	+1	+1	+1	+2

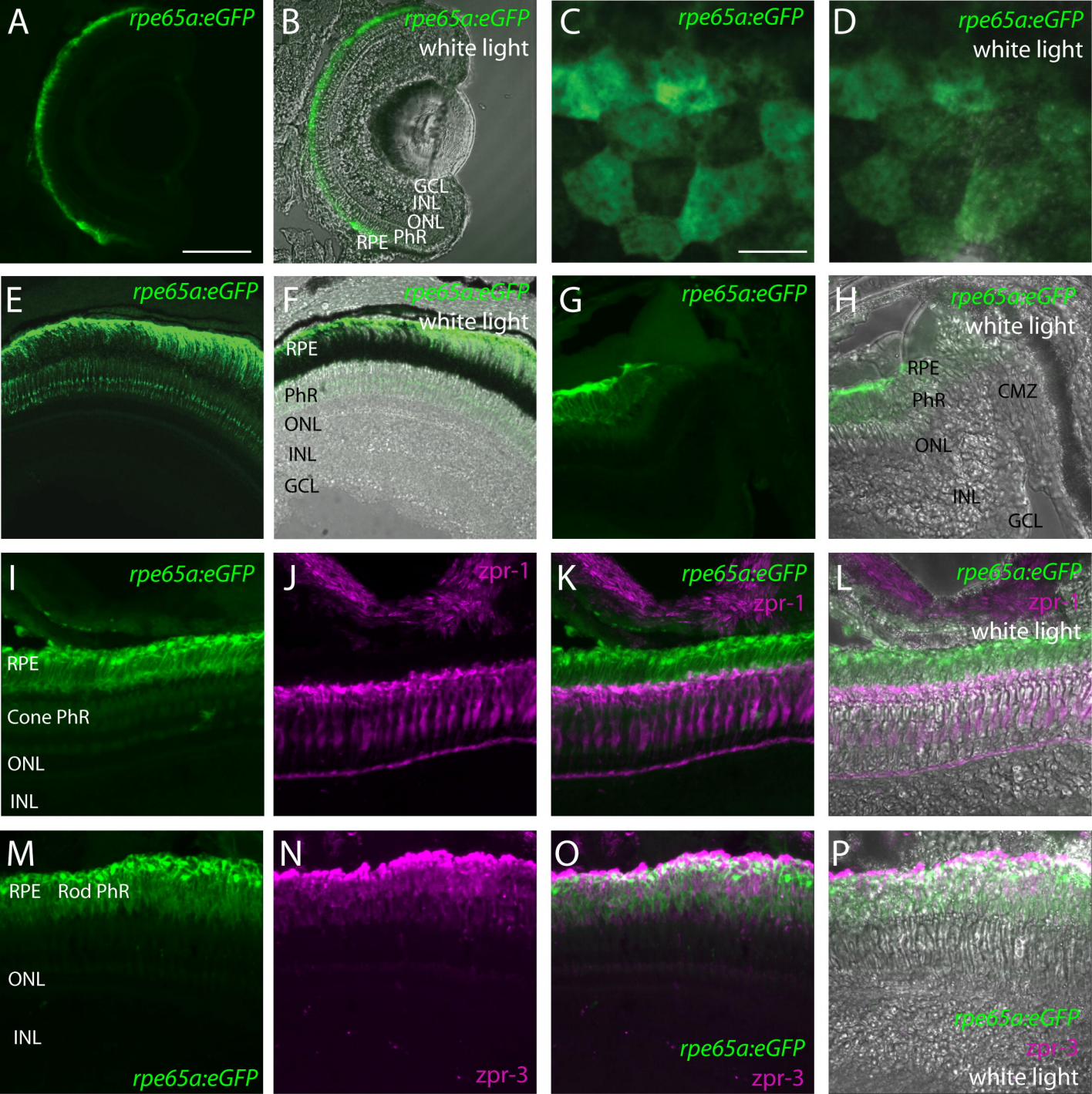
A
rpe65a:eGFP
B
rpe65a:eGFP
white light
GCL
INL
ONL
RPE
PhR
C
rpe65a:eGFP
D
rpe65a:eGFP
white light
E
rpe65a:eGFP
F
rpe65a:eGFP
white light
RPE
PhR
ONL
INL
GCL
G
rpe65a:eGFP
H
rpe65a:eGFP
white light
RPE
PhR
CMZ
ONL
INL
GCL
I
rpe65a:eGFP
RPE
Cone PhR
ONL
INL
J
zpr-1
K
rpe65a:eGFP
zpr-1
L
rpe65a:eGFP
zpr-1
white light
M
RPE
Rod PhR
ONL
INL
rpe65a:eGFP
N
zpr-3
O
rpe65a:eGFP
zpr-3
P
rpe65a:eGFP
zpr-3
white light

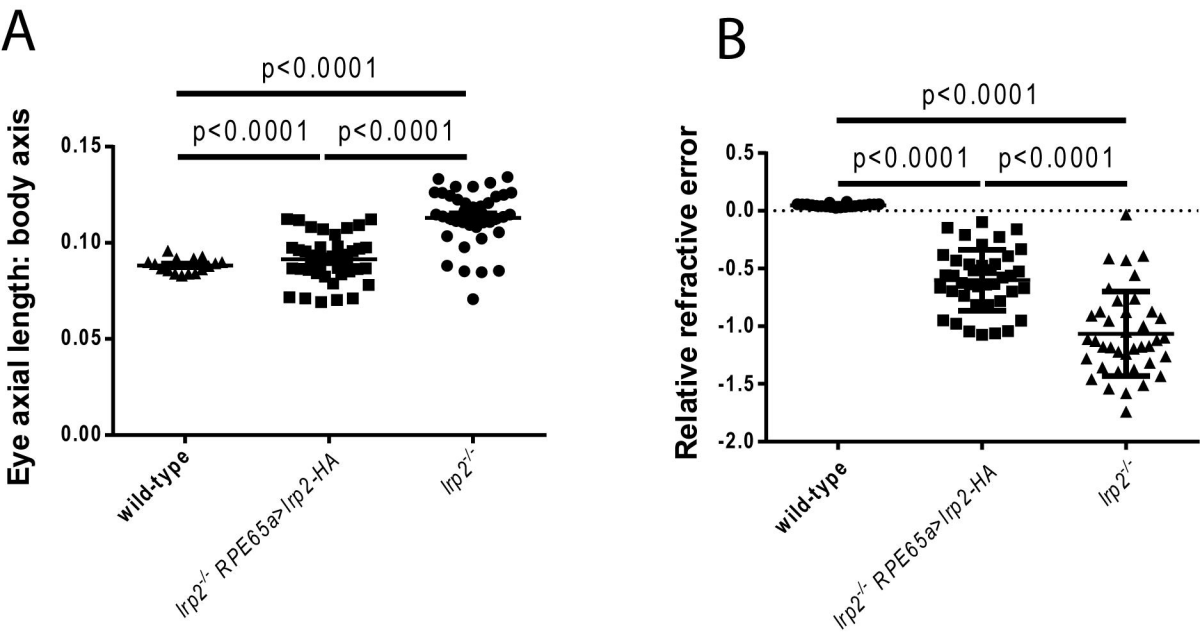
A
p<0.0001
p<0.0001
p<0.0001
Eye axial length: body axis
0.15
0.10
0.05
0.00
wild-type
lrp2-/- RPE65a>lrp2-HA
lrp2-/-
B
p<0.0001
p<0.0001
p<0.0001
Relative refractive error
0.5
0.0
-0.5
-1.0
-1.5
-2.0
wild-type
lrp2-/- RPE65a>lrp2-HA
lrp2-/-

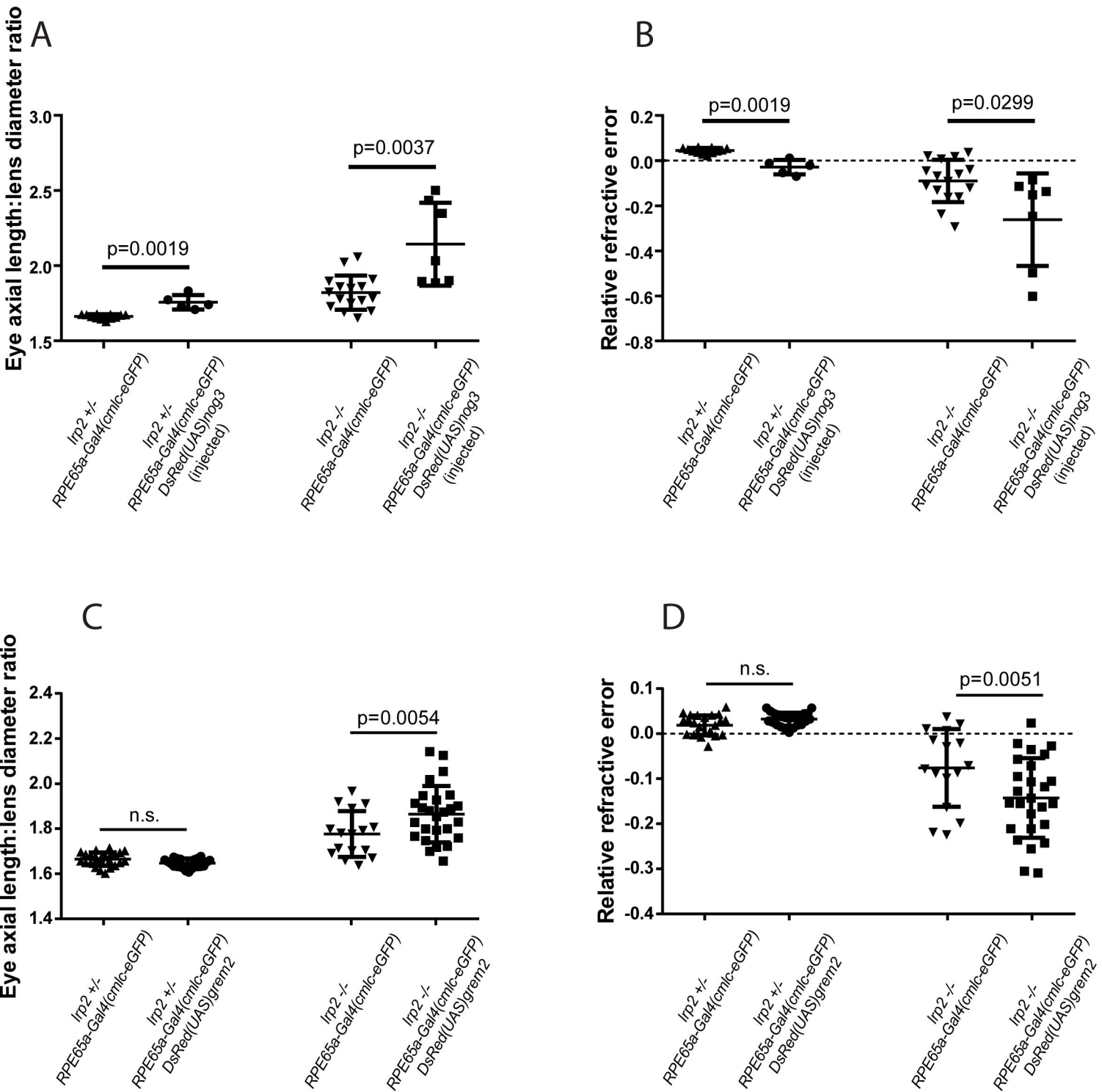
A
Eye axial length:lens diameter ratio
3.0
2.5
2.0
1.5
p=0.0019
p=0.0037
lrp2 +/- RPE65a-Gal4(cmlc-eGFP)
lrp2 +/- RPE65a-Gal4(cmlc-eGFP) DsRed(UAS)nog3 (injected)
lrp2 -/- RPE65a-Gal4(cmlc-eGFP)
lrp2 -/- RPE65a-Gal4(cmlc-eGFP) DsRed(UAS)nog3 (injected)
B
Relative refractive error
0.2
0.0
-0.2
-0.4
-0.6
-0.8
p=0.0019
p=0.0299
lrp2 +/- RPE65a-Gal4(cmlc-eGFP)
lrp2 +/- RPE65a-Gal4(cmlc-eGFP) DsRed(UAS)nog3 (injected)
lrp2 -/- RPE65a-Gal4(cmlc-eGFP)
lrp2 -/- RPE65a-Gal4(cmlc-eGFP) DsRed(UAS)nog3 (injected)
C
Eye axial length:lens diameter ratio
2.4
2.2
2.0
1.8
1.6
1.4
n.s.
p=0.0054
lrp2 +/- RPE65a-Gal4(cmlc-eGFP)
lrp2 +/- RPE65a-Gal4(cmlc-eGFP) DsRed(UAS)grem2
lrp2 -/- RPE65a-Gal4(cmlc-eGFP)
lrp2 -/- RPE65a-Gal4(cmlc-eGFP) DsRed(UAS)grem2
D
Relative refractive error
0.1
0.0
-0.1
-0.2
-0.3
-0.4
n.s.
p=0.0051
lrp2 +/- RPE65a-Gal4(cmlc-eGFP)
lrp2 +/- RPE65a-Gal4(cmlc-eGFP) DsRed(UAS)grem2
lrp2 -/- RPE65a-Gal4(cmlc-eGFP)
lrp2 -/- RPE65a-Gal4(cmlc-eGFP) DsRed(UAS)grem2

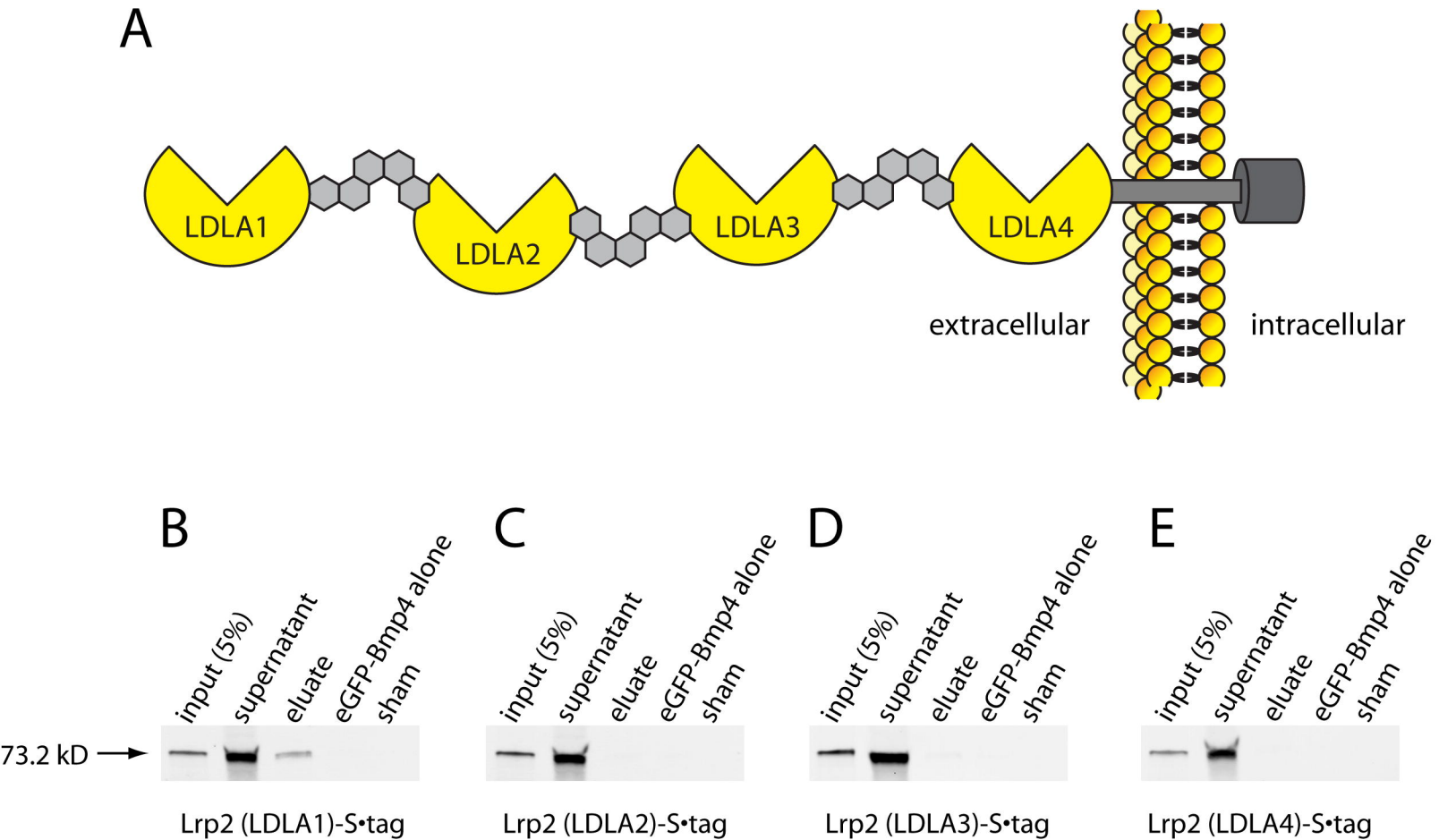
A
LDLA1
LDLA2
LDLA3
LDLA4
extracellular
intracellular
B
C
D
E
input (5%)
supernatant
eluate
eGFP-Bmp4 alone
sham
73.2 kD
Lrp2 (LDLA1)-S•tag
Lrp2 (LDLA2)-S•tag
Lrp2 (LDLA3)-S•tag
Lrp2 (LDLA4)-S•tag

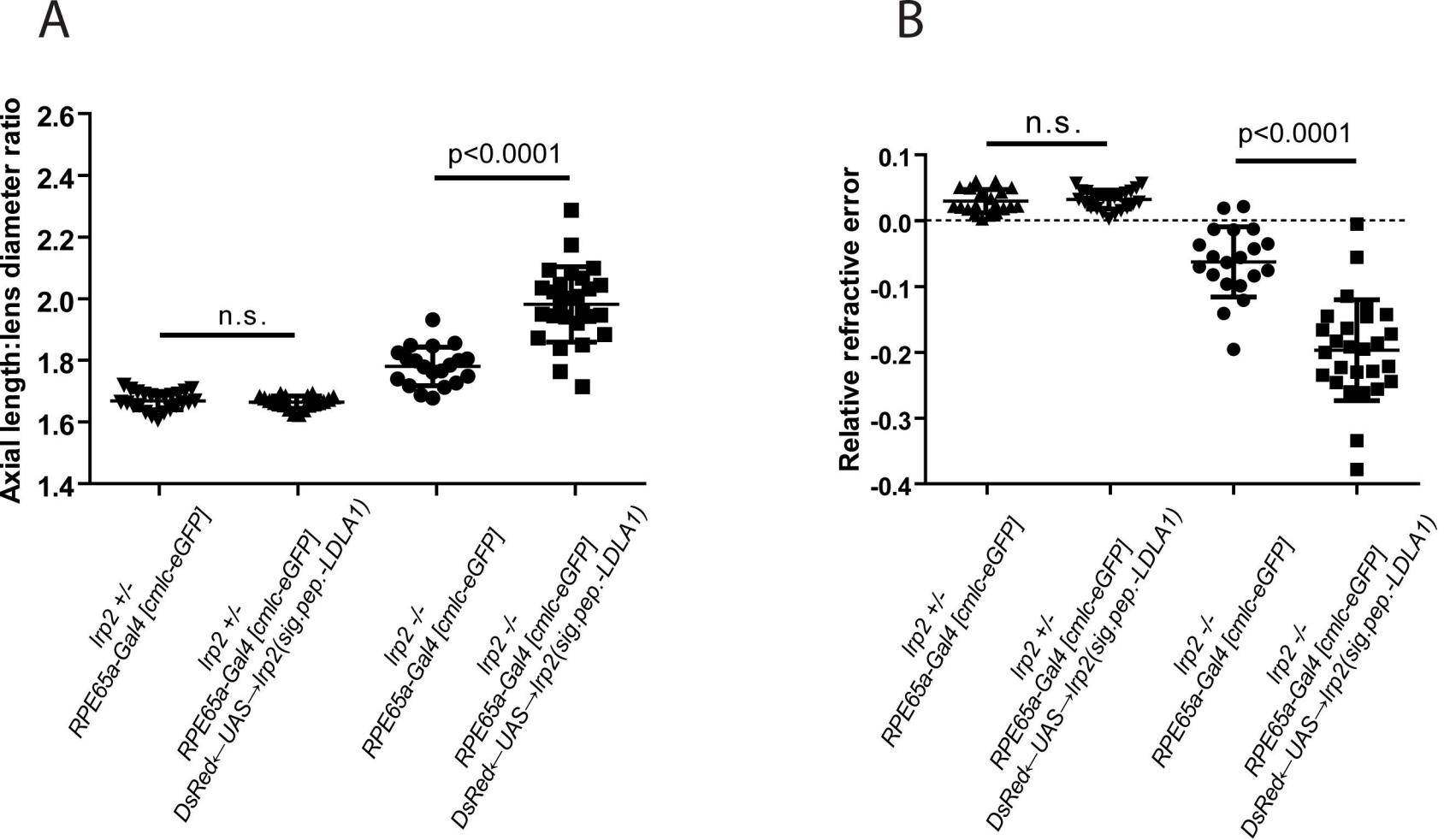
A
Axial length:lens diameter ratio
2.6
2.4
2.2
2.0
1.8
1.6
1.4
n.s.
p<0.0001
Irp2 +/-
RPE65a-Gal4 [cmlc-eGFP]
Irp2 +/-
RPE65a-Gal4 [cmlc-eGFP]
DsRed←UAS→Irp2(sig.pep.-LDLA1)
Irp2 -/-
RPE65a-Gal4 [cmlc-eGFP]
Irp2 -/-
RPE65a-Gal4 [cmlc-eGFP]
DsRed←UAS→Irp2(sig.pep.-LDLA1)
B
Relative refractive error
0.1
0.0
-0.1
-0.2
-0.3
-0.4
n.s.
p<0.0001
Irp2 +/-
RPE65a-Gal4 [cmlc-eGFP]
Irp2 +/-
RPE65a-Gal4 [cmlc-eGFP]
DsRed←UAS→Irp2(sig.pep.-LDLA1)
Irp2 -/-
RPE65a-Gal4 [cmlc-eGFP]
Irp2 -/-
RPE65a-Gal4 [cmlc-eGFP]
DsRed←UAS→Irp2(sig.pep.-LDLA1)

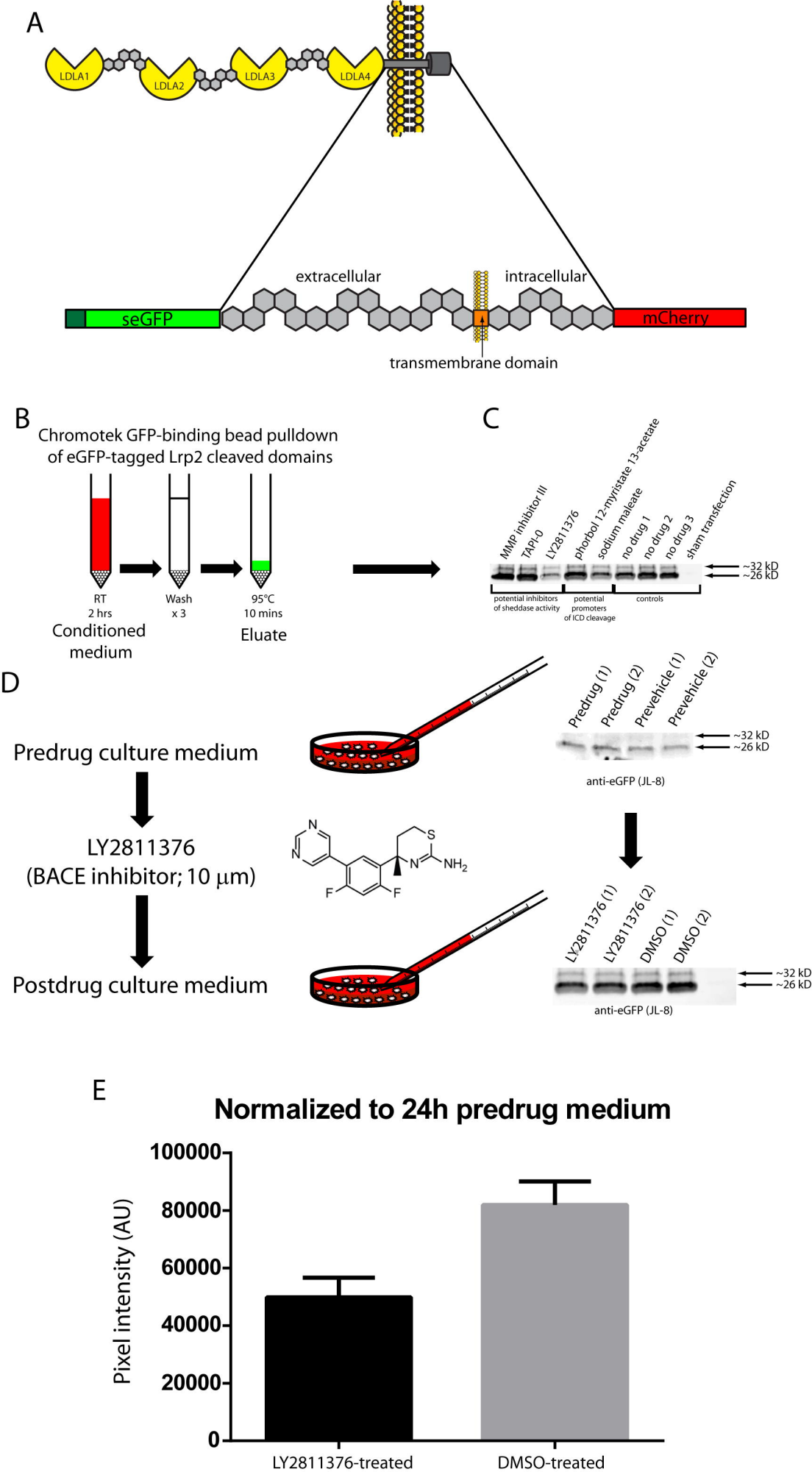
A
LDLA1
LDLA2
LDLA3
LDLA4
extracellular
intracellular
seGFP
mCherry
transmembrane domain
B
Chromotek GFP-binding bead pulldown
of eGFP-tagged Lrp2 cleaved domains
RT
2 hrs
Conditioned
medium
Wash
x 3
95°C
10 mins
Eluate
C
MMP inhibitor III
TAPI-0
LY2811376
phorbol 12-myristate 13-acetate
sodium maleate
no drug 1
no drug 2
no drug 3
sham transfection
~32 kD
~26 kD
potential inhibitors
of sheddase activity
potential
promoters
of ICD cleavage
controls
D
Predrug culture medium
LY2811376
(BACE inhibitor; 10 μm)
Postdrug culture medium
Predrug (1)
Predrug (2)
Prevehicle (1)
Prevehicle (2)
~32 kD
~26 kD
anti-eGFP (JL-8)
LY2811376 (1)
LY2811376 (2)
DMSO (1)
DMSO (2)
~32 kD
~26 kD
anti-eGFP (JL-8)
E
Normalized to 24h predrug medium
Pixel intensity (AU)
100000
80000
60000
40000
20000
0
LY2811376-treated
conditioned medium
DMSO-treated
conditioned medium

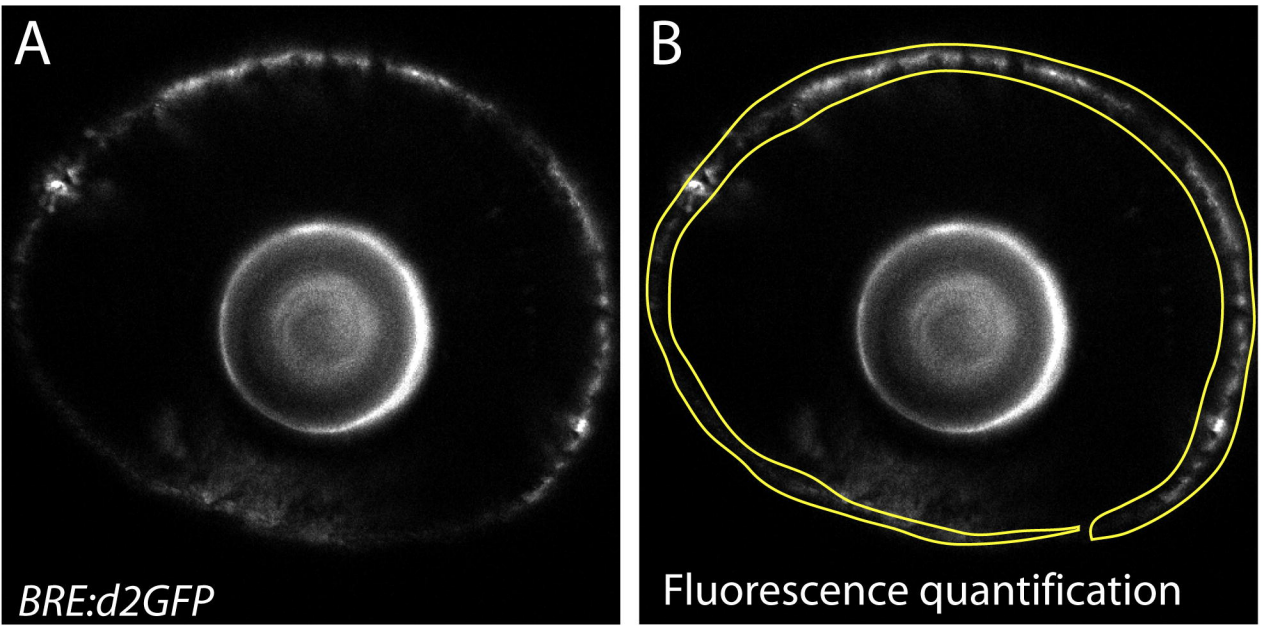
A
BRE:d2GFP

B
Fluorescence quantification

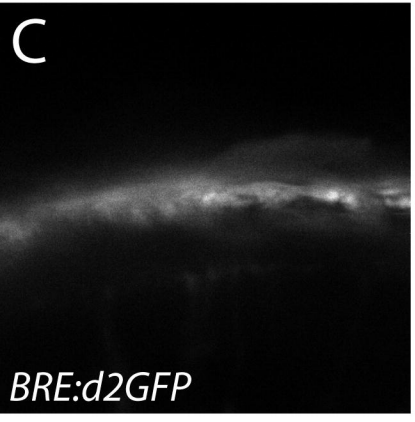
C
BRE:d2GFP

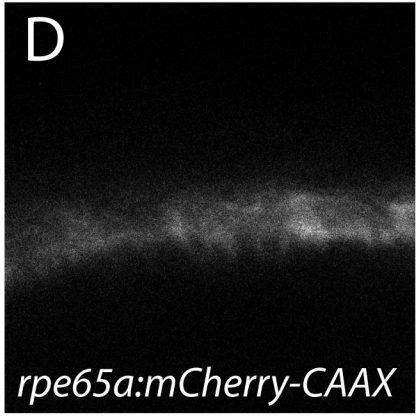
D
rpe65a:mCherry-CAAX

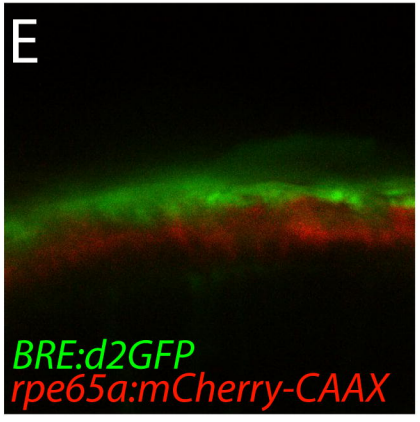
E
BRE:d2GFP
rpe65a:mCherry-CAAX

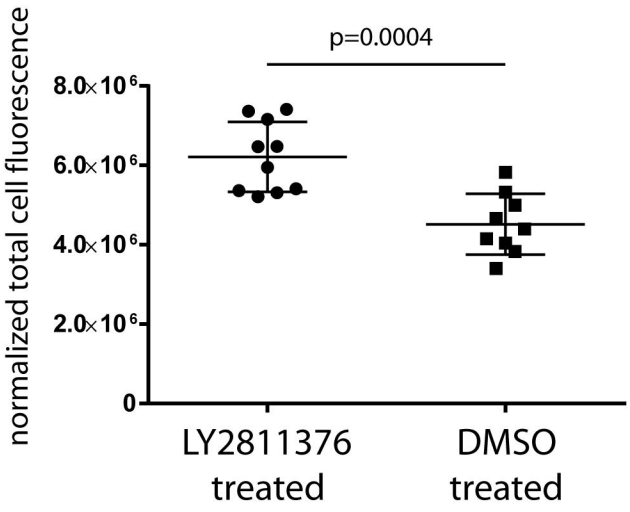
F
p=0.0004
normalized total cell fluorescence
8.0×10⁶
6.0×10⁶
4.0×10⁶
2.0×10⁶
0
LY2811376 treated
DMSO treated

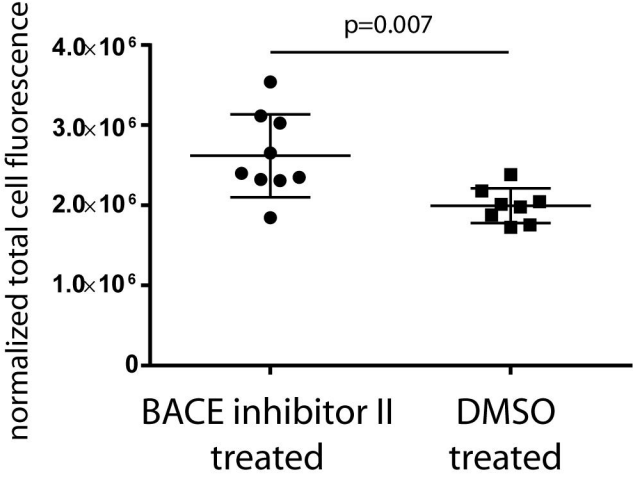
G
p=0.007
normalized total cell fluorescence
4.0×10⁶
3.0×10⁶
2.0×10⁶
1.0×10⁶
0
BACE inhibitor II treated
DMSO treated

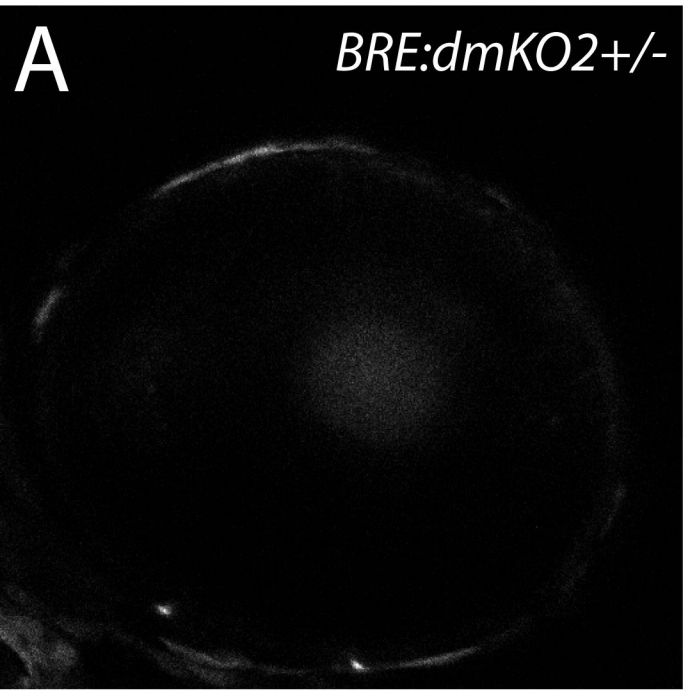
A
BRE:dmKO2+/-

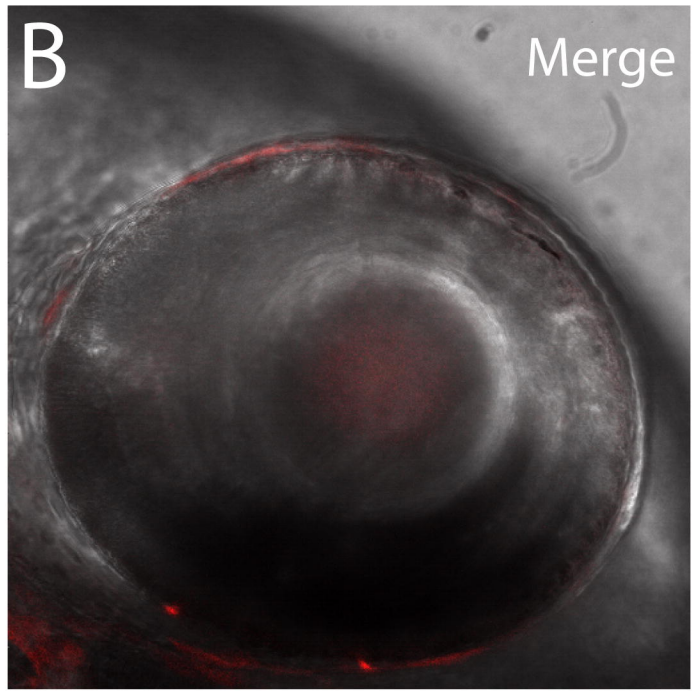
B
Merge

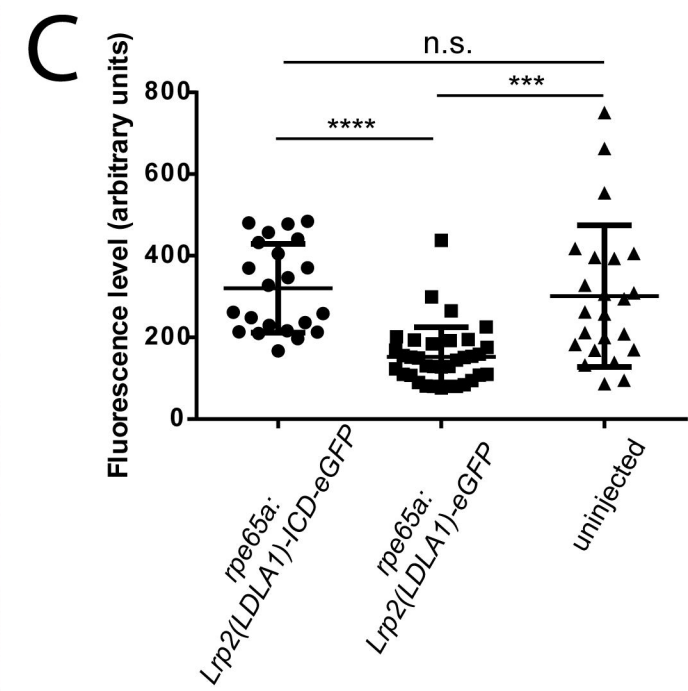
C
n.s.
***
****
800
600
400
200
0
Fluorescence level (arbitrary units)
rpe65a: Lrp2(LDLA1)-ICD-eGFP
rpe65a: Lrp2(LDLA1)-eGFP
uninjected

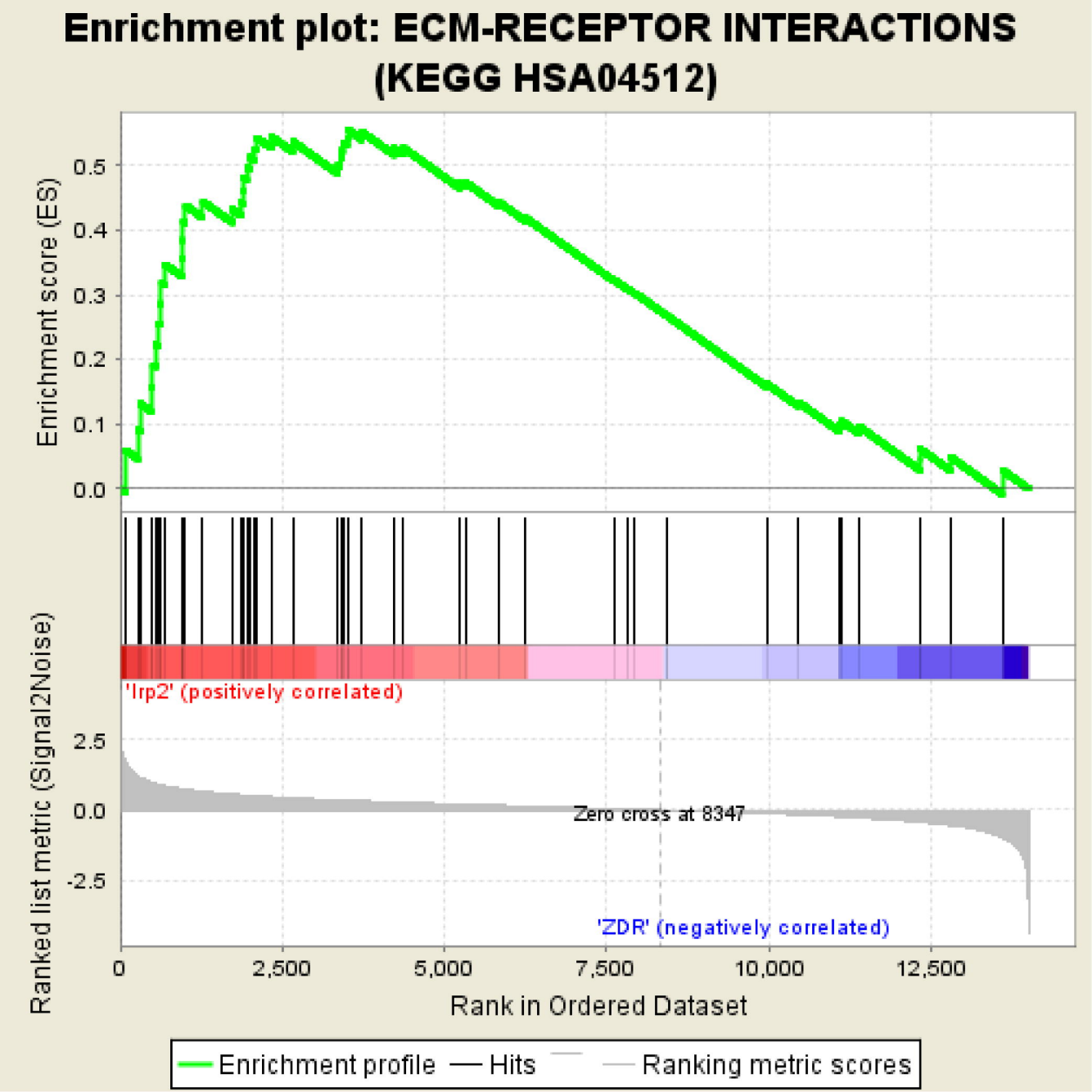
Enrichment plot: ECM-RECEPTOR INTERACTIONS (KEGG HSA04512)
Enrichment score (ES)
0.5
0.4
0.3
0.2
0.1
0.0
'Irp2' (positively correlated)
Ranked list metric (Signal2Noise)
2.5
0.0
-2.5
Zero cross at 8347
'ZDR' (negatively correlated)
0
2,500
5,000
7,500
10,000
12,500
Rank in Ordered Dataset
Enrichment profile
Hits
Ranking metric scores

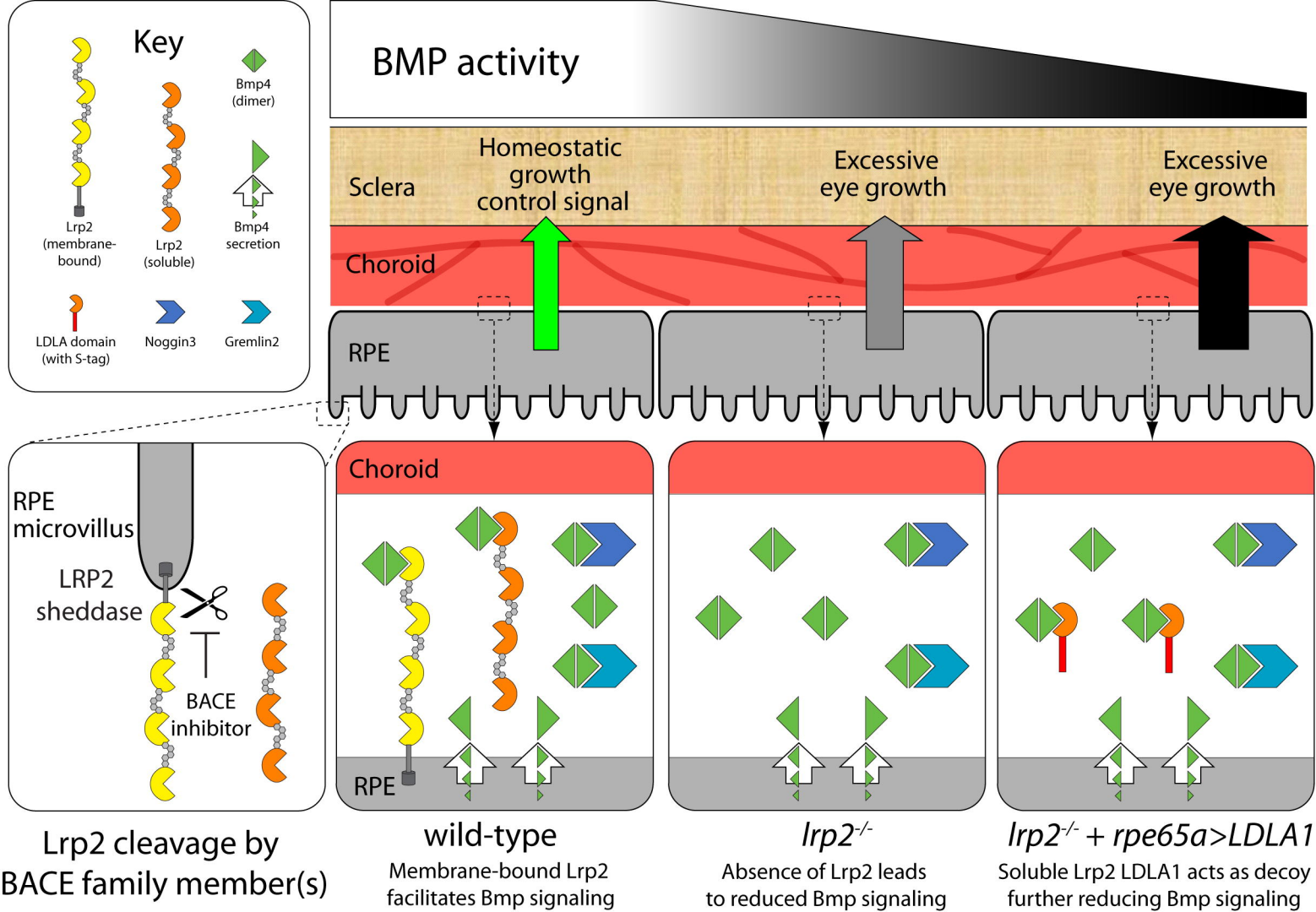
Key
Bmp4 (dimer)
Lrp2 (membrane-bound)
Lrp2 (soluble)
Bmp4 secretion
LDLA domain (with S-tag)
Noggin3
Gremlin2
BMP activity
Sclera
Homeostatic growth control signal
Excessive eye growth
Excessive eye growth
Choroid
RPE
RPE microvillus
LRP2 sheddase
BACE inhibitor
Choroid
RPE
Lrp2 cleavage by BACE family member(s)
wild-type
Membrane-bound Lrp2 facilitates Bmp signaling
lrp2-/-
Absence of Lrp2 leads to reduced Bmp signaling
lrp2-/- + rpe65a>LDLA1
Soluble Lrp2 LDLA1 acts as decoy further reducing Bmp signaling